KTH Aeronautical
and Vehicle Engineering

Interaction between ultrasonic waves and nonlinear cracks and interfaces

Milan Poznić

Licentiate Thesis

TRITA-AVE 2005:43
ISSN 1651-7660

Postal address	*Visiting Address*	*Telephone*	*Fax*	*Internet*
KTH MWL SE-100 44 Stockholm, Sweden	Teknikringen 8 Stockholm	+46 8 790 6000	+46 8 790 9290	www.kth.se

Abstract

The need to develop nonlinear inspection techniques for detection and characterization of partially closed cracks in fluid-filled pipes is twofold. First, conventional linear techniques lack the sensitivity to small material changes, such as those at the onset of a stress-corrosion crack. Second, they can not provide information on whether the crack is surface-breaking or not when the ligament separating the crack from the inner surface of the pipe is small compared to the wavelength of the inspecting wave.

An experimental investigation into the linear reflection and generation of the second harmonic component following the incidence of an ultrasonic wave onto a dry or water-confining interface between elasto-plastic steel-steel surfaces in contact introduces this thesis. The results with water-confining interfaces indicate that current models not accounting for the liquid-mediated forces between the solid surfaces cannot explain the experimental results presented here. In addition, the level of second harmonic generation by these interfaces offers support for the development of inspection techniques which exploit such wave phenomena for the detection of partially closed and dry, or nearly open and water-trapping stress-corrosion surface-breaking cracks.

A theoretical model describing the nonlinear scattering of acoustic waves by surface-breaking cracks with faces in partial contact is presented next. Both linear and nonlinear response of the crack are shown to be the largest for a shear vertical (SV) wave incident on the surface containing the crack at an angle just above the critical angle for longitudinal waves.

Finally, a novel ultrasonic method which provides information on whether a fracture reaches the surface of the hosting component or is entirely embedded within its bulk has been modelled and its optimal experimental set-up examined. The main assumption of the model is that water carried by pressurized pipes infiltrates and fills a surface-breaking crack, while a subsurface crack is dry. The model simulates an inspection in which the modulation technique is employed and the surface hosting the crack is not accessible. A ratio, R, constructed with signals recorded in backscattering configuration during a modulation cycle, is examined and shown to provide a clear criterion to distinguish subsurface from surface-breaking cracks when a shear vertical wave at 45 degree incidence is employed as a probe.

Acknowledgements

The research presented in this licentiate thesis was performed at the Marcus Wallenberg Laboratory for Sound and Vibration Research (MWL), Department of Aeronautical and Vehicle Engineering, KTH. The Swedish Centre for Nuclear Technology (SKC) provided the gratefully acknowledged research funding.

First of all I would like to thank my supervisor D.Sc. Claudio Pecorari for valuable, lively discussions, and guidance, and most of all his deep engagement as a researcher. Many thanks to the steering group at SKC for their support and interesting meetings.

A warm thank must be dedicated to Professor Anders Nilsson for his invaluable support to my family.

I also want to thank my colleges and friends at the department for a nice time and interesting discussions, especially Mathieu Boué from whom I've been given many good comments and valuable recommendations, both in this work and life in general. Further more I want to thank Kent Lindgren and Danilo Prelević, for their help with the experiments.

Thanks Pia for standing by my side at all times and together with Luka bringing a smile at my face, wherever I am ☺ Thanks also for all the valuable scientific discussions which many times brought daylight to darkness.

Stockholm, December, 2005

Milan Poznić

Thesis

The thesis presented consists of an introduction to the research field and the following three papers:

Paper A

C. Pecorari and M. Poznic, "On the linear and nonlinear acoustic properties of dry and water-confining elasto-plastic interfaces", to appear in *Proceedings of the Royal Society A: Mathematical, Physical and Engineering Sciences*.

Paper B

C. Pecorari and M. Poznic, 2005 "Nonlinear acoustic scattering by a partially closed surface-breaking crack", *J. Acoust. Soc. Am.* 117, 592-600.

Paper C

M. Poznić and C. Pecorari, "So, . . . is this a surface-breaking crack ?", submitted to the *J. Mechanics of Materials and Structures.*

Contribution from the author of this thesis:

Paper A:	Development of the experimental setup, participated in the experiments
Paper B:	Development of the simulation tool, performed simulations, analyzed the results
Paper C:	Development of the simulation tool, performed simulations, analyzed the results

Contents

1 Introduction

Stress-corrosion cracks (SCCs) are a constant threat to the integrity of engineering structures such as pipes carrying crude oil or other highly pollutant substances in refineries and chemical plants. Several instances of stress-corrosion cracking in critical components in nuclear power plants have also been reported. This is the case, for example, of the reactors Oconee 1, 2, and 3, Arkansas 1, and Davis Besse in the US, where most cracks were found to be axially oriented, and, thus, less prone to cause catastrophic failure of the system. However, circumferential cracks within the base material were also discovered. Such defects are of much greater concern to the integrity of the component, to the extent that a revision of the recommended inspection procedures was required by the US Nuclear Regulatory Commission (NRC) after they were found. Large SCCs have been recently discovered also in Swedish nuclear power plants (Ringhals 3 and 4). They were axially oriented and embedded within the weld materials.

SCCs are the result of the combined action of tensile stresses due to the plant's operating conditions or residual stresses introduced by welding, and the corrosion produced by the harsh surrounding environment. They are often found in regions proximal to the inner surface of the pipe, sometimes being entirely embedded within the material, more often reaching the surface of the component. The latter are the most dangerous because of their accelerated growth induced by the penetration of water within the fracture. Water penetration occurs because surface-breaking cracks (SBCs) are held open during operation by tensile stresses and the internal pressure to which water is subjected may reach values up to 70 atmospheres in water boiling reactors and 160 atmospheres in pressurized water reactors.

Due to the random nature of the corrosion process, the surfaces of SCCs are nonconforming to each other, and when they are brought together by a compressive stress field, or by the release of the stresses generated while the component is in operation, they form a random pattern of isolated contacts across the cracked area. In addition, since the nonconformity of the crack's faces prevents its complete closure (see figure 1), the likelihood of finding a liquid layer trapped between the crack faces is very high, even when the fracture is partially closed during routine inspections.

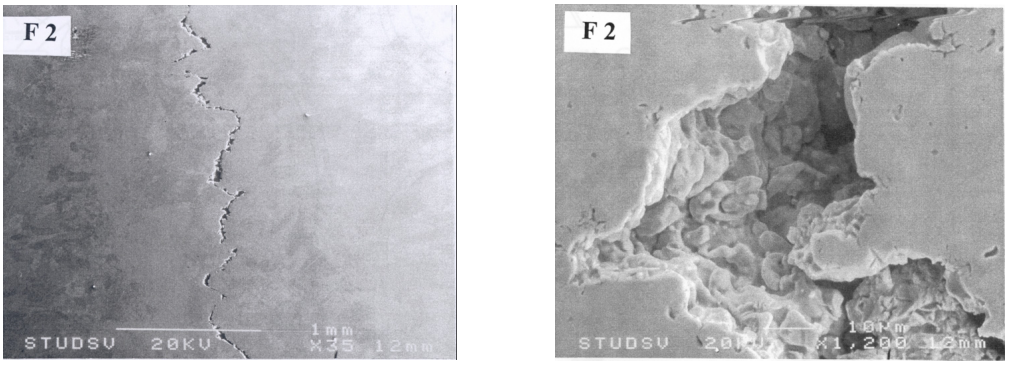

Figure 1 *Two images at different magnification of the same SSC*

Nuclear power plants undergo periodic nondestructive inspections aiming at assessing their structural integrity. Conventional ultrasonic techniques employed in such circumstances exploit linear wave scattering phenomena. These techniques may perform poorly if a crack is partially closed, or fluid filled, or surrounded by material with coarse microstructure. Partial closure and water penetration weaken the acoustic contrast of a fracture by enhancing the transmission of the inspecting wave. Coarse microstructure increases the background noise, which tends to hide weak signals.

Additional problems presented by conventional techniques concern their ability to estimate the size of SCCs, and characterize cracks as being surface-breaking or subsurface, when the ligament which separates the crack from the surface is small compared to the diameter of the inspecting beam. An example of this problem is provided by the experience at Ringhals 4 mentioned above, in which cracks that were judged to be entirely contained within the material (sub-surface) by ultrasonic techniques, were found to be surface-breaking by the following metallurgical investigation.

In laboratory experiments, material components containing partially closed cracks have been shown to respond to an external large dynamic perturbation in a nonlinear manner (see Solodov [1998] and Solodov *et al.* [2002] for a few examples). For instance, when insonified by a harmonic wave, the spectrum of the acoustic response of a cracked sample, has been shown to display higher-order harmonic components, which are not found in samples without cracks.

Similarly, if a component containing a partially closed crack is tested simultaneously by two harmonic waves of frequencies f_1 and f_2, with $f_1 >> f_2$, signals are generated within the sample, which contain side-band components at frequencies $f_1 \pm f_2$. These, again, are not found in the acoustic fields generated by scattering events in material components without cracks. An even richer phenomenology can be observed when the amplitude of the excitation is increased beyond the threshold value at which clapping between the crack's faces is activated (Solodov and Korshak [2002]). For example, the generation of subharmonic components, which is the first step towards a chaotic regime of vibration, can be observed by progressively increasing the excitation amplitude. Nonlinear effects caused by the dissipation of the acoustic energy have also been reported in experiments conducted on cracked glass samples (Zaistev *et al.* [2002]).

The experiments mentioned above are often performed with continuous waves at frequencies that are well below the MHz range, that is to say, the wavelength of the waves propagating within the inspected component is of the order of several centimetres. Furthermore, the dimensions of the samples are finite and stationary sensors are employed in these experiments. For these reasons, the results proving the nonlinearity of cracked samples cannot be reproduced by the experimental set-up currently in use in routine inspections of power plant's components.

In this thesis, problems concerning the broader issues of detection and characterization of partially closed cracks in components of nuclear power plants by means of nonlinear methods are addressed. In particular, the nonlinear acoustic properties of steel-steel interfaces are experimentally investigated with the aim of establishing their strength as sources of nonlinear acoustic signals. Furthermore, models of both linear and nonlinear backscattering by dry and water-confining SBCs and subsurface cracks (SSC) have been developed. The aim of the latter is to provide some guidance to the development of novel techniques to be employed in power plant inspections.

2 Summary of the papers

2.1 Paper A

An ongoing research activity at The Marcus Wallenberg Laboratory for Sound and Vibration Research (MWL) concerns itself with the nonlinear interaction between ultrasonic waves and interfaces formed by rough surfaces in contact. Recent results have been summarized in two earlier articles, in which the interaction between asperities has been assumed to be either purely elastic (Pecorari [2003]), or determined also by forces of adhesion (Pecorari [2004]). *Paper A* reports an experimental investigation into the generation of the first and second harmonic component by interfaces formed by rough steel surfaces in contact, the latter being treated as distributions of springs with normal and tangential stiffness, K_N and K_T, respectively (Baik and Thompson [1984], Pecorari [2003] among the many publications on the subject). Within the framework of the spring model, the dynamic response of an imperfect interface to an incident ultrasonic wave is described by the following quasi-static boundary conditions,

$$\sigma_{xx}^{+} = K_N \, \Delta u \,, \tag{1}$$

$$\sigma_{xy}^{+} = K_T \Delta v \,, \tag{2}$$

which are accompanied by the continuity of the relevant components of the total stresses across the interface. In the above equations σ_{ij}^{+} is the *ij* stress component on the positive side interface, and Δu and Δv are the displacement jumps in the normal and transverse direction, respectively. The value of the interface stiffness can be recovered from the assessment of the reflection coefficient, R, of a bulk wave at normal incidence, $R = -1 \big/ \left(1 - 2jK^{*}\right)$, where $K^{*} = K \big/ \left(\omega Z\right)$. In this expression, K is the physical interface stiffness, $\omega = 2\pi f$ is the angular frequency of the incident wave, and Z is the medium acoustic impedance appropriate for the bulk incident wave.

The experiments have been motivated by the following specific goals:

i. to establish the most relevant mechanism(s) in the generation of the second harmonic wave by comparing the experimental findings with available theoretical predictions (Pecorari [2003 and 2004], Kim *et al*. [2004]);

ii. to investigate the effect of a fluid layer confined between two solid rough surfaces on the linear and nonlinear response of an interface;

iii. to assess the dynamic range of the nonlinear signal over the noise threshold which is intrinsic to the instrumentation available to us.

Figure 1 illustrates the geometry of the samples forming the interface, as well as additional details concerning the position of the transducer and the loading configuration.

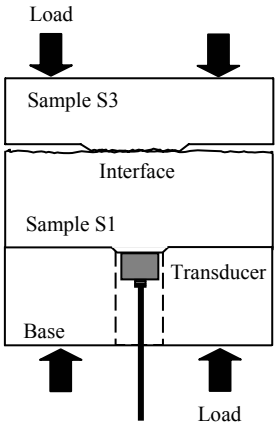

Figure 1. *Detailed sketch of the interface-forming materials and of the transducer's location.*

Figure 2 shows the nonlinear dependence of the normalized stiffness K^* on the interfacial pressure as the latter is increased up to 250 MPa, and then decreased until the unloaded configuration is reached. These results have been obtained using an interface formed by samples having an rms roughness, R_q= 0.25 μm and 0.1 μm. They are referred to as S_1 and S_3, respectively, in figure 1. The hysteretic loop formed the values of K^* is due to plastic deformation occurring at the load-bearing asperities during a loading cycle. Additional experimental results with different surfaces are also reported in *Paper A*. They confirm the expectation that hysteresis decreases as the surfaces get smoother, and that the nonlinearity of a dry interface is determined by that of the force-displacement relation together with the non-uniform distribution of the asperities.

When water is added to the interface, the normal stiffness, K_N, is determined by the mechanical contacts considered earlier and by the stiffening liquid. At the onset of mechanical contact, when no external pressure has yet been applied, the contribution from the water layer can be modelled by the ratio Λ/d_o, where Λ is the non-zero Lame' constant of the liquid, and d_o is the initial aperture of the interface.

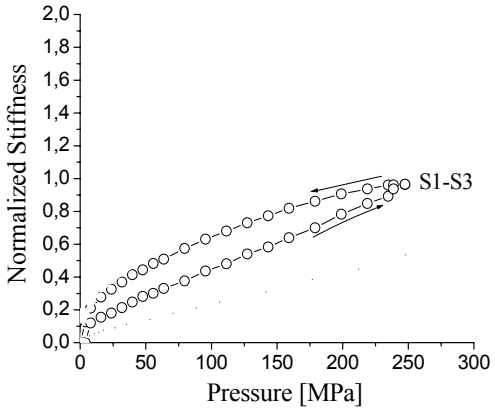

Figure 2. *Interface normalized stiffness versus applied pressure for the interface considered. The data have been acquired during the loading and unloading phases of the same cycle.*

The remaining part of the stiffness, ΔK_N, varies with pressure and is illustrated in figure 3. Note the large increase in ΔK_N at pressure values below 5MPa, which could not be seen in the case of a dry interface (see figure 2). This suggests that other mechanisms, which are discussed in the paper, play a significant role in the description of the interfacial stiffness.

The generation of the second harmonic by dry and water-confining interfaces is illustrated in figure 4 a) and b), respectively. Both figures show that the level of the signal is significantly higher than the noise generated by the instrumentation, which is about -80 dB. Of interest if the large nonlinear response of a water-confining interface when no pressure is applied to it, but mechanical contact between the surfaces has already been established. These results suggest that the presence of fluid within the fracture may allow nonlinear methods to be used for detection purposes under conditions in which the nonlinear response of dry crack would not be too weak.

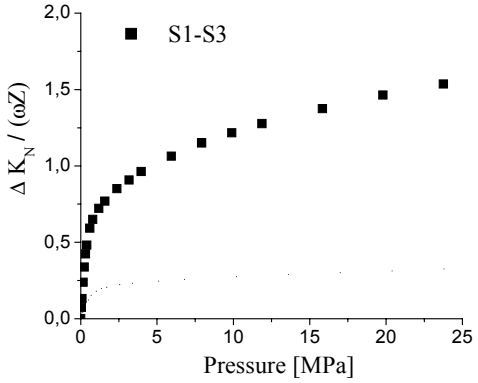

Figure 3. *Variation of the normalized stiffness of a water-confining interface versus applied pressure for the interface considered in the previous figure. The data are acquired during loading.*

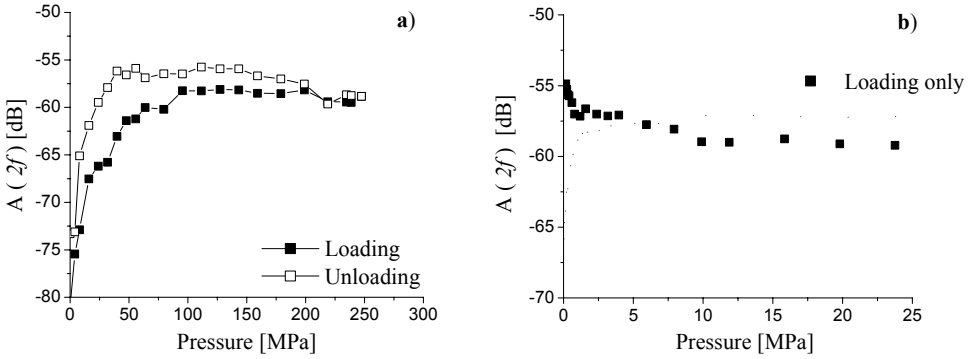

Figure 4. *Amplitude of the second harmonic component generated by the interface as function of the applied pressure for: a) a dry interface and b) a fluid-containing interface. The data have been acquired during the loading and unloading phases of the same cycle.*

2.2 Paper B

Paper B presents a theoretical model of linear and nonlinear backscattering by partially closed, dry SBCs. The aim of this work is to investigate the experimental configuration which maximizes the nonlinear response. Scattering of waves by open SBCs has been treated first by Achenbach *et al*. [1980] and Mendelsohn *et al*. [1980], while Pecorari [2001] developed the theory to account for partial closure of the defect. In *Paper B* the model is further extended to include nonlinear spring boundary conditions ([Pecorari, 2003]). The scattering problem is solved by using perturbation theory up to the first order in a small parameter which controls the generation of the second harmonic. The dependence of the amplitude of backscattered second harmonic on the incident wave's polarization, on the interface stiffness, on the crack depth, and on the coordinates of the observation point are investigated. The spatial evolution of the linear and nonlinear components of the scattered field is also evaluated up to distances of the order of ten wavelengths of the incident wave from the crack.

The most favourable configuration to detect a surface-breaking crack by means of a bulk wave is found to be the one in which a shear-vertical waves is used as probe (figure 5). In the simulations the frequency of he incident wave is f = 5MHz. Figure 6 shows the dependence of

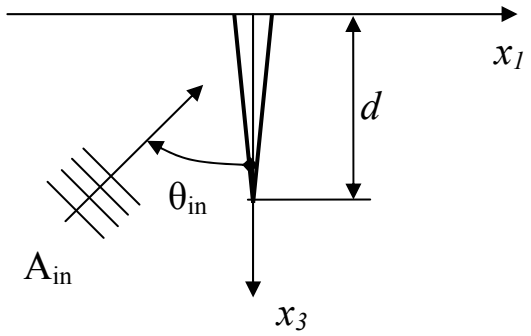

Figure 5. *Schematic representation of the surface-breaking crack and of the coordinate system used in the model*

the amplitude the backscattered second harmonic component on the angle of incidence for several values of the distance of the observation point from the surface hosting the crack. The

latter has a normalized size, $D = k_L d = 0.5$, where k_L is the wave number of a longitudinal wave, and a normalized stiffness $K_N^* = 1.95$. These results indicate that the largest response is obtained when the angle of incidence exceeds the critical angle of the longitudinal wave, θ_L = 33º in steel, by a few degrees. For a different material the critical angle of the longitudinal wave will change and therefore also the best configuration. The same results yield for the linear response.

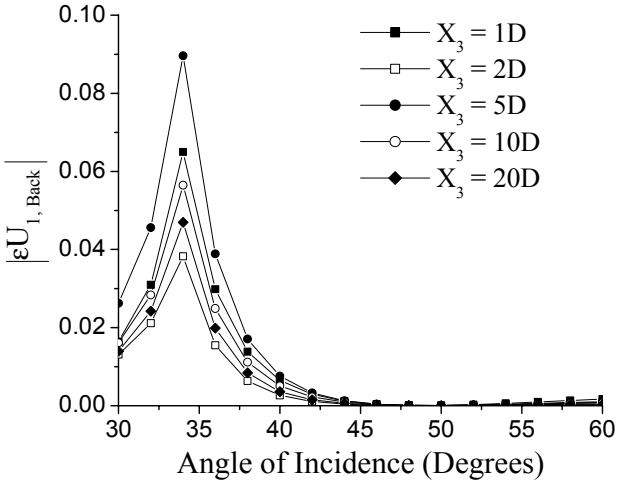

Figure 6. *Normalized backscattered horizontal displacement of the nonlinear field versus the angle of incidence for increasing values of the normalized depth of the observation point. The latter is measured in terms of normalized crack's depth, D= k_Ld. The normalized crack's depth is D = 0.5, while* $K_N^* = 1.95$ *and* $\varepsilon = 0.144$.

2.3 Paper C

Paper C focuses on modelling a novel approach to distinguish SBCs from SSCs. The proposed method exploits the distinctive pressure dependence of the normal stiffness of surface-breaking fractures which are filled with water (see *Paper A*). A low frequency, high amplitude pressure field, $P(t) = \Delta P \sin(\Omega t)$, which modulates the stiffness of the crack, is applied to the crack, while a high frequency, ultrasonic wave is used to monitor the current state of the defect by monitoring its backscattered field. By using the peak-to-peak amplitude,

or any other feature of the backscattered signal which reflects the variation of the crack state, the following ratio is constructed: $R = \left(B^{-} - B^{+} \right) \Big/ B_o$, where $B^{-,+}$ are the features of interest measured when the crack is most open (-) or closed (+), respectively, and B_o refers to the crack state in its rest condition. Note that the ratio R is independent of the amplitude of the incident wave, and, thus, conveys information which depends on the intrinsic properties of the defect but not on the intensity of the inspecting wave. In this work the technique is investigated theoretically in order to define the most suitable experimental configuration to solve the problem of interest. Thus, ultrasonic wave scattering by both dry SSCs and fluid filled SBCs is simiulated. The modulation technique has been introduced by Xiao and Nagy [1998], and was further developed by Rokhlin *et al.* [2004], Kim *et al.* [2004], and Kazakov *et al.* [2002].

The scattered field is evaluated theoretically following the same formulation as in *Paper B* but with the following two additions. First, the defect is non-uniformly closed in order to incorporate crack tip closure (see for example Newman [2003]), and second, the crack can be sub-surface. The non-uniform closure is introduced in the model by varying the applied pressure, *P(y)*, along the defect as described by the following equations which are given for a SSC (see figure 7),

$$P(y) = P_{tip} \exp\left[(y-b) \big/ \ell \right], \quad (a+b)/2 \le y \le b, \tag{3}$$

$$P(y) = P_{tip} \exp\left[-(y-a) \big/ \ell \right], \quad a \le y \le (a+b)/2. \tag{4}$$

In eq. (3-4), P_{tip} is the pressure at the crack tips and ℓ is the decay length which controls the spatial extent of the tip closure. The pressure distribution on a surface-breaking crack is obtained from eq. (3-4) by letting $a = 0$. A schematic representation of the method is given in figure 8.

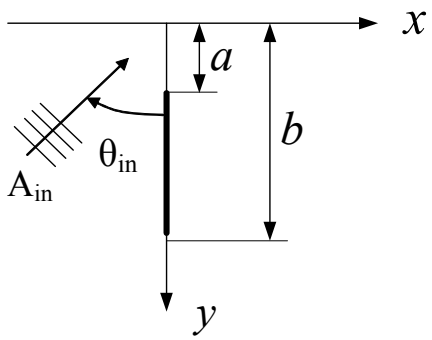

Figure 7. *Geometry of the material system and of its defect. The material system occupies the halfspace y > 0. For a surface-breaking crack a = 0.*

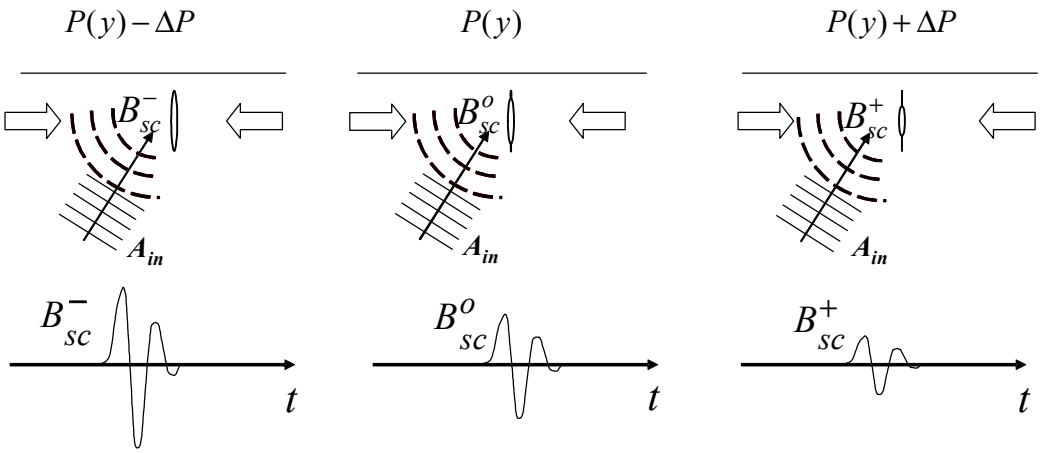

Figure 8. *Schematics of the simulated modulation experiment illustrating the relationship between the state of the crack and the signal backscattered by it during a cycle of the modulation.*

The results reported in this section are from simulations considering shear vertical incidence at an angle of θ_{in} = 45º. The frequency of the inspecting wave is f = 2.2 MHz. Figure 9 shows the ratio, R, versus the non-dimensionl crack size, $k_T d$, for a surface-breaking, fluid filled crack with ℓ = 0.1 mm and P_{tip} = 5 MPa and 70 MPa. The observation point lies at a distance of about 30 shear wavelengths (about 40 mm) from the surface of the halfspace. Similar simulations

have been performed on dry SSCs and figure 10 shows the results for 3 different sizes of the ligament, a, and P_{tip} = 70 MPa.

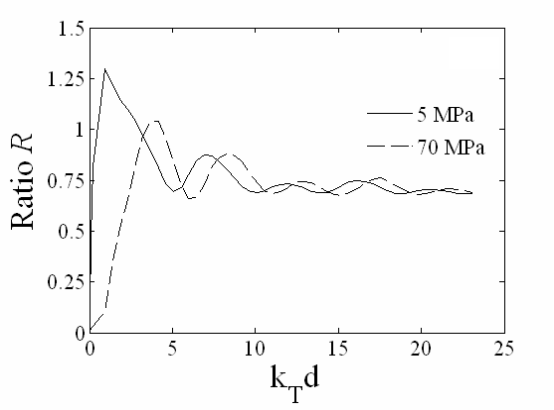

Figure 9. *Ratio, R, versus nondimensional crack size $k_T d$ for values of the pressure at the crack tip equal to 5 MPa and 70 MPa. The pressure distribution decays exponentially from the crack tip with a characteristic length ℓ=0.1 mm. The surface-breaking crack is water-confining.*

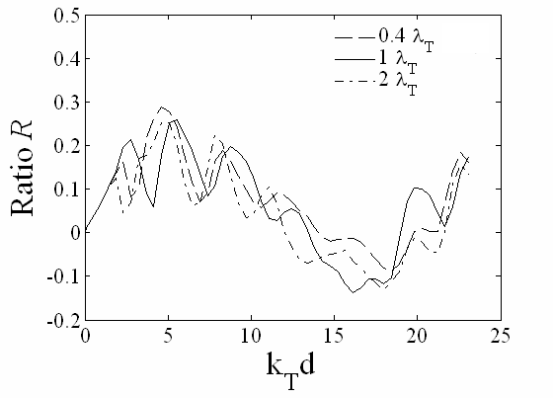

Figure 10. *Ratio, R, versus nondimensional crack size $k_T d$ for values of the ligament equal to $0.4\lambda_T$, $1\lambda_T$, and $2\lambda_T$. The pressure distribution decays exponentially from the crack tip with a characteristic length ℓ =0.1 mm. P_{tip} = 70 MPa.*

A comparison between figure 9 and 10 show that the magnitude of the ratio R in the case of a fluid filled SBC always remains significantly higher than for a dry SSC, independently of the defect size. Note that the results presented here are the worse case for this particular

configuration; larger decay lengths yield an even better contrast between the two. This observation suggests that R may serve as a criterion to distinguish SBCs from SSCs. *Paper C* also shows that the criterion holds for values of θ_{in} = 40º and 50º.

Although not reported here, the behaviour of the ratio R has been examined also for θ_{in} = 33º, the critical angle for the longitudinal wave, and found not to yield a clear criterion to discern the two types of cracks. Similar negative results have been obtained with longitudinal waves at 45 degrees, 60 degrees and 85 degrees incidence.

3 Concluding Remarks

This work has investigated the potential of nonlinear techniques as diagnostics tools to enhance the detection and characterization of partially closed cracks in nuclear power plants.

Experiments on interfaces formed by two rough surfaces in contact have shown that the nonlinearity arising from the elasto-plastic contacts between the asperities determines the strength of the second harmonic generation. An even more pronounced nonlinearity can be seen as fluid is added to the interface. Contrary to dry interfaces, a large generation of the second harmonic could be measured already at low contact pressures. This unpredicted behaviour can not be explained by the nonlinear bulk stiffness of fluid layers in combination with asperities in contact alone. Other mechanisms, likely to be linked to the confinement of the fluid, must be included. Most importantly, this feature is expected to extend the range within which nonlinear methods could be used to detect also defects which are weakly closed.

A theoretical model which describes the nonlinear backscattering from partially closed cracks has been developed and the experimental configuration which provides the highest sensitivity to small surface-breaking cracks has been identified. It has been also shown that, contrary to current practices, this configuration should be used even to detect small surface-breaking cracks when linear backscattering is employed.

Finally, a method to distinguish subsurface cracks from those reaching the inner surface of a fluid-filled pipe has been theoretically investigated. To this end, the modulation technique has been used which exploits the sensitive dependence of the stiffness of a fluid-filled, surface-breaking crack on the applied pressure, and the effect of the latter on the linear backscattering by this type of defects when they are non-uniformly closed. The experimental configuration has been optimized to provide the best criterion to separate subsurface from surface-breaking cracks.

4 Future work

The main objective of the work which follows this thesis is the validation of the model's predictions concerning the ability of the modulation technique to distinguish SBCs from SSCs. A suitable experimental setup, based on the theoretical predictions, will be designed and constructed, and experiments on model defects will be performed. A second issue to be experimentally investigated concerns the detection of small partially closed cracks by means of the generation of the second harmonic.

REFERENCES

Achenbach, J.D., Keer, L.M., and Mendelsohn, D.A., "Elastodynamic analysis of an edge crack", *J. Appl. Mech*. **47**, 551-556 (1980).

Baik, J.M. and Thompson, R.B., "Ultrasonic scattering from imperfect interfaces: a quasi-static model", *J. Non-Destruct. Eval*. **4**, 177-196 (1984).

Kazakov, V.V., Sutin, A., and Johnson, P.A., "Sensitive imaging of an elastic nonlinear wave-scattering source in a solid", *Appl. Phys. Lett.* **81**, 646-648 **(**2002).

Kim, J.-Y., Baltazar, A., and Rokhlin, S.I., "Ultrasonic assessment of rough surface contact between solids from elastoplastic loading-unloading hysteresis cycle" *J. of Mech. Phys. Solids* **52**, 1911-1934 (2004).

Mendelsohn, D.A., Achenbach, J.D., and Keer, L.M., "Scattering of elastic waves by a surface-breaking crack", *Wave Motion* **2**, 277-292 (1980).

Newman, J.A., Riddell, W.T., and Piascik, R.S., "Analytical and experimental study of near-threshold interactions between crack closure mechanisms", NASA/TM-2003-211755,ARL-TR-2774 (2003).

Pecorari, C., "Scattering of a Rayleigh wave by a surface-breaking crack with faces in partial contact", *Wave Motion* **33**, 259-270 (2001).

Pecorari, C., "Nonlinear interaction of plane ultrasonic waves with an interface between rough surfaces in contact", *J. Acoust. Soc. Am.* **113**, 3065-3072, (2003) and references therein.

Pecorari, C., "Adhesion and nonlinear scattering by rough surfaces in contact: Beyond the phenomenology of the Presach-Mayergoyz framework", *J. Acoust. Soc. Am.* **116**, 1938-1947 (2004).

Rokhlin, S.I., Wang, L., Xie, B., Yakovlev, V.A., and Adler, L., "Modulated angle beam ultrasonic spectroscopy for evaluation of imperfect interfaces and adhesive bonds", *Ultrasonics* **42**, 1037-1047 (2004).

Solodov, I.Y., "Ultrasonics of non-linear contacts: propagation, reflection and NDE applications", *Ultrasonics* **36**, 383-390 (1998).

Solodov, I.Y. and Korshak, B.A., "Instability, chaos, and 'memory' in acoustic wave crack interaction", *Phys. Rev. Lett*. **88**, 014303 (2002).

Solodov, I.Y., Krohn, N., and Busse, G., "CAN: an example of non-classical acoustic nonlinearity in solids", *Ultrasonics* **40**, 621-625 (2002).

Xiao, H. and Nagy, P.B., "Enhanced ultrasonic detection of surface-breaking cracks by laser-induced crack closure", *J. Appl. Phys*. **83**, 7455-7460 (1998).

Zaistev, V.Y., Gusev, V., and Castagnede, B., "Luxenburg-Gorky effect retooled for elastic waves: a mechanism and experimental evidence", *Phys. Rev. Lett*. **89**, 105502 (2002).

Zaistev, V.Y., Gusev, V., and Castagnede, B., "Observation of the 'Luxenburg-Gorky' effect for elastic waves", *Ultrasonics* **40**, 627-631 (2002).

PAPER A

On the linear and nonlinear acoustic properties of dry and water-confining elasto-plastic interfaces

Claudio Pecorari, Milan Poznic
Marcus Wallenberg Laboratory
Royal Institute of Technology
10044 Stockholm, Sweden

Abstract

An experimental investigation into the linear reflection and generation of the second harmonic component following the incidence of an ultrasonic wave onto a dry or water-confining interface between elasto-plastic steel-steel surfaces in contact is presented. The results on dry interfaces show that, although the theoretical models currently used to estimate the stiffness of such interfaces constitute a valid framework, the statistics of asperities in contact requires further development to account for the effects of the elasto-plastic deformation. Similarly, the results with water-confining interfaces indicate that current models not accounting for the liquid-mediated forces between the solid surfaces cannot explain the results presented here. In fact, the experimental evidence is interpreted as suggesting that structural repulsive forces may be responsible for the observed phenomena. Finally, the level of second harmonic generation for these interfaces offers support for the development of inspection techniques which exploit such wave phenomena for the detection of partially closed and dry, or nearly open and water-trapping stress-corrosion surface-breaking cracks.

Keywords: confined water, elasto-plastic interface, ultrasonic waves

To appear in Proceedings of the Royal Society, A (Mathematical, Physical and Engineering Sciences)

1. Introduction

In view of their potential for accelerated growth, stress corrosion cracks (SCCs) constitute a major danger to the structural integrity of nuclear power plant components and of other systems subjected to similar environmental factors and operating conditions. SCCs are generated by the combined action of stress fields that are caused by the conditions under which the component operates, or residual stresses, and of corrosion due to the harsh surrounding environment. Due to the random nature of the corrosion process, the surfaces of SCCs are nonconforming to each other. Thus, when they are brought together by a compressive stress field, or by the release of the tensile stresses generated while the component is in operation, the surfaces form a random pattern of isolated contacts across the crack area. In addition, since the nonconformity of the crack's faces prevents its complete closure, the likelihood of finding a liquid layer trapped between the crack faces is not negligible. Indeed, since the water pressure in a duct connected to a reactor pressure vessel is of the order of 70 atmospheres, it is nearly certain that all cracks which open to the internal surface of such a pipe will be filled with liquid.

In this communication, the results of an investigation on the linear reflectivity and the generation of the second harmonic component by dry and water-confining nonlinear interfaces formed by rough steel surfaces in elasto-plastic contact are reported. The relevance of this subject to the nondestructive detection and evaluation of SCCs stems from the role played by this type of interfaces as prototypical models for partially closed stress-corrosion cracks. In particular, the investigation of the nonlinear response of partially closed surfaces is believed to constitute a necessary step towards the development of potentially new techniques which, operating in the frequency domain, provide the required sensitivity and spatial resolution for the detection of SCCs (see Pecorari & Poznic (2005) for a discussion of this issue).

Interfaces affected by damage, or formed by rough surfaces in partial contact have been shown to respond in nonlinear fashion when they are excited by an incident acoustic wave. A host of experimental investigations have explored this phenomenon in some of its most salient features. On the other hand, few theoretical studies have attempted to

link the acoustic macroscopic nonlinear response of interfaces to their structural properties at a microscopic scale. The interested reader is referred to Pecorari (2003) and Pecorari (2004) for a review of the relevant literature. Not discussed in these references is a novel and rather pragmatic approach by Biwa *et al*. (2004), in which the pressure dependence of the interfacial stiffness is modeled as a power law containing two parameters to be determined by a best-fitting procedure. Although attractive for its simplicity, this approach fails to provide any physical insight into the mechanisms which determine the response of an interface to an incident wave. In fact, at the center of Biwa *et al*.'s work is the assumption according to which the dynamic stiffness, K_{dyn}, of the interface is identified with the derivative of the pressure, *P*, with respect to the relative approach between the surfaces, δ, $K_{dyn} = \partial P / \partial \delta$. While this is legitimate for a perfectly elastic interface, there is sufficient evidence showing that the dynamics of important interfacial systems dramatically depart from that implied by this assumption. For instance, adhesion forces have been predicted to yield a hysteretic behavior of the dynamic interfacial stiffness which cannot be described by a simplistic power law (Pecorari, 2004). A second important example, which is discussed later in detail for its relevance to the subject of this work, is provided by an interface between surfaces in elasto-plastic contact (Kim, Baltazar, & Rokhlin, 2004). Therefore, if a proper understanding of the wave scattering by surfaces in partial contact is to be achieved, the development of models based on well-established physics at the microscopic scale appears to be the only way forward.

The present experimental investigation into the generation of the second harmonic component by interfaces formed by rough steel surfaces in contact has been motivated by the following specific goals:

i. to assess the dynamic range of the nonlinear signal over the noise threshold which is intrinsic to the instrumentation available to us;

ii. to establish the most relevant mechanism(s) in the generation of the second harmonic wave by comparing the experimental findings with available theoretical predictions (Pecorari, 2003 and 2004, Kim *et al*., 2004);

iii. to investigate the effect of a fluid layer confined between two solid rough surfaces on the nonlinear response of an interface.

In the course of the investigation, the experimental results obtained on the dependence of the interface reflectivity on the applied pressure have also prompted a re-examination of the physical mechanisms controlling the linear response of the interfaces entrapping a liquid layer.

The content of this communication is organized as follows. In the next section, the experimental results are presented together with a description of the set-up and materials employed in the investigation. Next, these results are discussed in view of the current understanding of wave scattering phenomena by surfaces in contact. In particular, features which the models fail to reproduce are examined to find aspects of the latter in need of development. Finally, a brief summary of the main results ends this communication.

2. Experimental Results

Experimental Set-Up and Materials

The experimental set-up consists of a computer-controlled, high-power tone-burst generator (SNAP MarkV, RITEC Inc.) which excites a commercial transducer (Panametrics V541, ½" diameter) with a train of 24 sinusoidal cycles at a frequency $f = 5$ MHz . All the measurements are carried out in reflection mode. Thus, the same transducer is used both as a transmitter and as a receiver. After passing a diplexer (see Figure 1a), the signal returning from the transducer is sent either directly to the SNAP system for the detection of the first harmonic component, or goes through a high-pass filter, which suppresses the first harmonic component, and a preamplifier (40 dB) for the detection of the second harmonic. A further amplification of 30 dB by the receiving electronics within the SNAP system determines the amplitude of the time-domain signals which, after being time-averaged, are displayed and Fourier analyzed by a digital oscilloscope (Tektronix TDS 5052).

Figure 1b illustrates the geometry of the samples forming the interface, as well as additional details concerning the positioning of the transducer and the loading configuration.

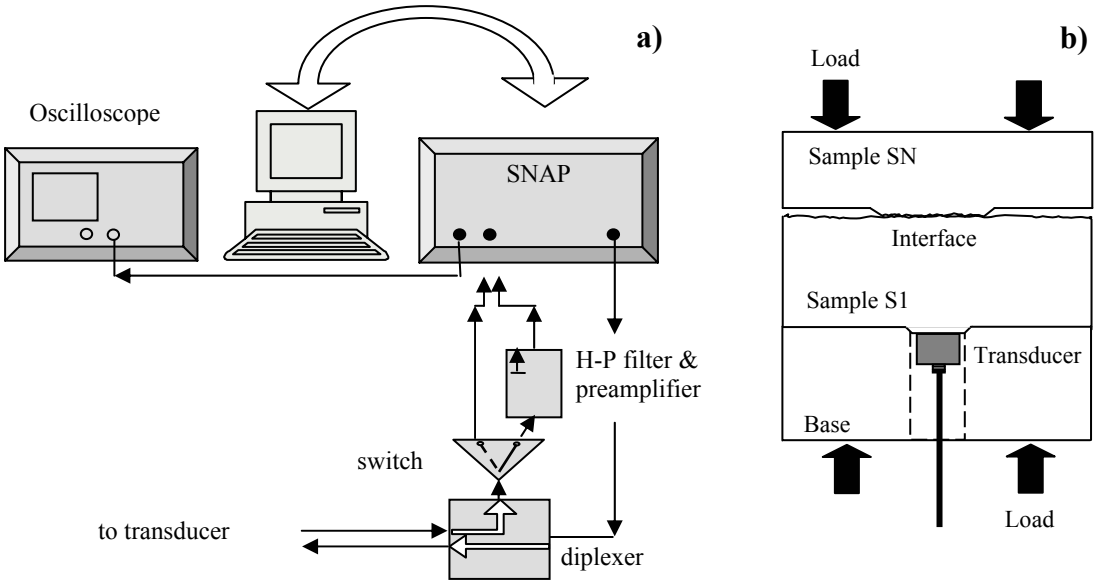

Figure 1. *a) Block diagram of the experimental set-up; b) detailed sketch of the interface-forming materials and of the transducer's location*.

Four steel samples have been employed in this work. Of these, the sample S1 has been used in all the measurements as the medium supporting the propagation of the incident and reflected waves. The thickness of this sample is of 85 mm, which sets the position of the receiver in the far-field region of the inspecting beam. The surface of the sample S1 which is in contact with the transducer is shaped so that the sensor sits on the face of a truncated cone, while the remaining surface is in contact with an auxiliary steel sample (the base – see Figure 1b) which transfers the load from the MTS loading machine to the interface through the sample S1. The purpose of this arrangement is to avoid the interface between the transducer and S1 being affected by the applied load. Of the remaining three samples, S2 and S4 offer a nominal contact area with a radius of 30 mm, and S3 with a radius of 20 mm. The surfaces of the samples were lapped on a table designed for this purpose and by using pastes of various degrees of coarseness. Their rms surface roughness values, R_q, which are given in Table I, have been obtained by averaging three measurements carried out on 3 mm long, one-dimensional profiles, and, thus, they underestimate the actual rms roughness of the two-dimensional surfaces on two accounts. First, being one-dimensional, such profiles do not generally pass over the peaks of the two-dimensional asperities. Second, the length of the trace works as a cut-off limit of a high pass filter. Therefore, low frequency components of the profile which

may be present in these surfaces do not contributed to the estimate of the rms roughness. Nonetheless, the R_q values are reported here as a way to classify the surfaces involved in this investigation. In addition to the previous remark, it is necessary to mention that, among these surfaces, that of the sample S2 is to be considered as an anomalous case. In fact, as illustrated by the profiles gathered on this sample, its surface shows long smooth segments separated by deep grooves produced during polishing. Such grooves, although isolated, are sufficiently dense to affect the estimate of the rms roughness value for this surface, but not the dynamics of the interface formed by it. In other words, without the contribution from the deep groves, the measurements of the rms roughness would have likely provided a rather smaller value for this sample. Table I provides also an estimate of the rms wavelength of the profile, λ_q, defined by the ratio $\lambda_q = 2\pi R_q / \Delta_q$, where Δ_q is the rms slope of the profile.

	S1	S2	S3	S4
R_q (μm)	0.25	< 0.14	0.1	1.5
λ_q (μm)	9.9	12	6.1	20

Table I. *Measured rms roughness and rms wavelength of the profile of the four surfaces used in the experiments.*

2.1 Dry Steel-Steel Interface

Three interfaces with different rms roughness values were investigated by combining sample S1 with the remaining three. To establish the dynamic range of the nonlinear response of each interface, external pressures ranging from zero up to values approaching the yield stress of the material have been employed. Prior to recording the data which are presented next, each interface was loaded once up to 250 MPa, the maximum value of the load used in this work, to verify that the system would return to the initial condition once the load was removed.

Figure 2a illustrates the behavior of the amplitude of the reflected first harmonics, $A(f)$, during a complete loading cycle. The variation of this quantity is largest for the combination of the surface S1-S2, the latter of which previous remarks have characterized as the smoothest of all four surfaces. The area of the hysteretic loop associated with the

smoothest interface is shown to be the smallest, consistent with the expectation that the smoother the interface, the closer its behavior to perfectly elastic. However, departures from the expected behavior are possible as shown by the comparison between the loops associated with the interfaces S1-S3 and S1-S4. A possible explanation for such a result may be the increased hardening of the higher asperities of the rougher surface following the loading cycle preceding the data acquisition.

From these data, the reflection coefficient of a longitudinal wave at normal incidence, $R = -1/\left(1 - 2jK^*_{N,0}\right)$, can be recovered, and used to evaluate the normalized interface stiffness, $K^*_{N,0} = K_{N,0}/\left(\omega Z_L\right)$. In this expression, $K_{N,0}$ is the physical interface stiffness, $\omega = 2\pi f$ is the angular frequency of the incident wave, and Z_L is the medium longitudinal acoustic impedance. Similar results have been reported earlier by other authors (see, for example, Drinkwater *et al.* (1996)) for interfaces between aluminum samples, but only recently Kim *et al*. (2004) have provided the first sound physical model for this type of observations. In addition, these authors have discussed a method which allows several interface parameters to be recovered from a suitable analysis of the experimental data gathered during the loading phase of a cycle. These parameters play crucial roles in defining both the topography and the mechanical properties of the interface.

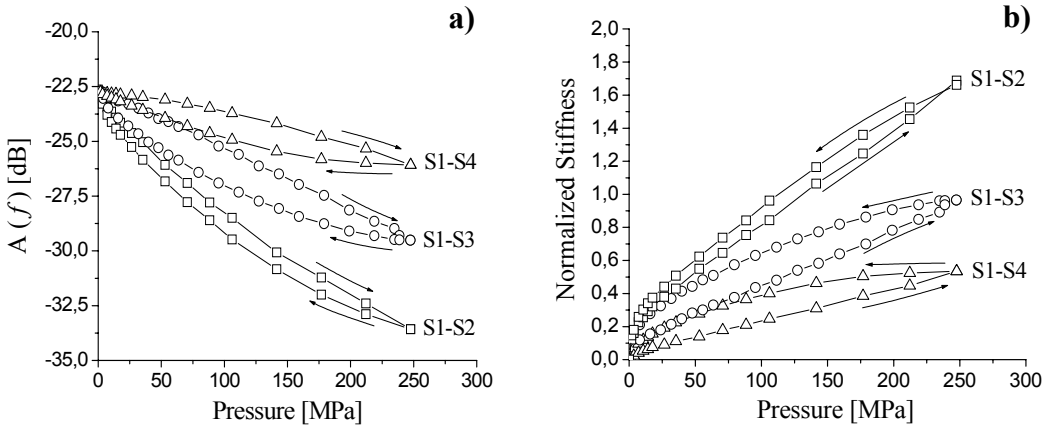

Figure 2. *a) Amplitude of the linearly reflected component by the dry interfaces versus applied pressure; b) interface normalized stiffness versus applied pressure for the three interfaces considered in the previous figure. The data have been acquired during the loading and unloading phases of the same cycle.*

Extending this investigation to the nonlinear dynamics of the interfaces of interest, Figures 3a-c show the behavior of the amplitude of the second harmonic component, $A(2f)$, which is generated by each interface during the same loading cycles examined in the previous figure. The modulus of $A(2f)$ is shown to rise at a rate that is greatest for the smoothest interface S1-S2. It also reaches a maximum which, as predicted by the theory, is higher than that of the other two interfaces and is followed by a slow descent. In other words, the smaller the rms roughness, the higher the maximum nonlinear response of the interface (Pecorari, 2003). In the case of the other two interfaces, S1-S3 and S1-S4, the rate of increase and the maximum magnitude reached by the amplitude of the second harmonic decreases with increasing rms roughness. Of relevance for its implications on the detection of partially closed cracks, the dynamic range is shown to exceed 20 dB over the threshold of the noise in all three cases, which sits approximately at a value of – 80 dB for the instrumentation used in this work. Therefore, the dynamic range increases with decreasing roughness. As in the linear case, the nonlinear properties of the interface S1-S2 are shown to differ only slightly from those expected from a perfectly elastic interface although the variation consistently indicates that the response is larger during unloading, especially at smaller pressure values (Fig. 3a). This observation is confirmed by the following two figures (Fig. 3b and 3c) in which the nonlinear generation during the unloading portion of the cycle is seen to dominate over that during the loading part, the difference between the two being greater than 5 dB and approaching 10 dB at low values of the applied pressure.

Considering that the time-domain signal which is examined for its content at twice the frequency of the incident wave undergoes a pre-amplification of 40 dB with respect to the linear signal, the results of Fig. 2a and Fig. 3 illustrate that the nonlinear response is 70 to 80 dB below the fundamental component. However, for a realistic evaluation of the relative magnitude of these two signals, one should keep in mind the
effect of the transducer response which is expected to heavily penalize the second harmonic with respect to the first one. To provide the reader with a rough estimate of the transducer's sensitivity loss as a function of the frequency, a test was performed in which the sensor was excited with two trains of 20 cycles; each train had the same amplitude, and the frequency was equal to 5 MHz and 10 MHz, respectively. The signals reflected

by the stress-free surface of sample S1 were recorded and found to be about 25 dB lower at 10 MHz.

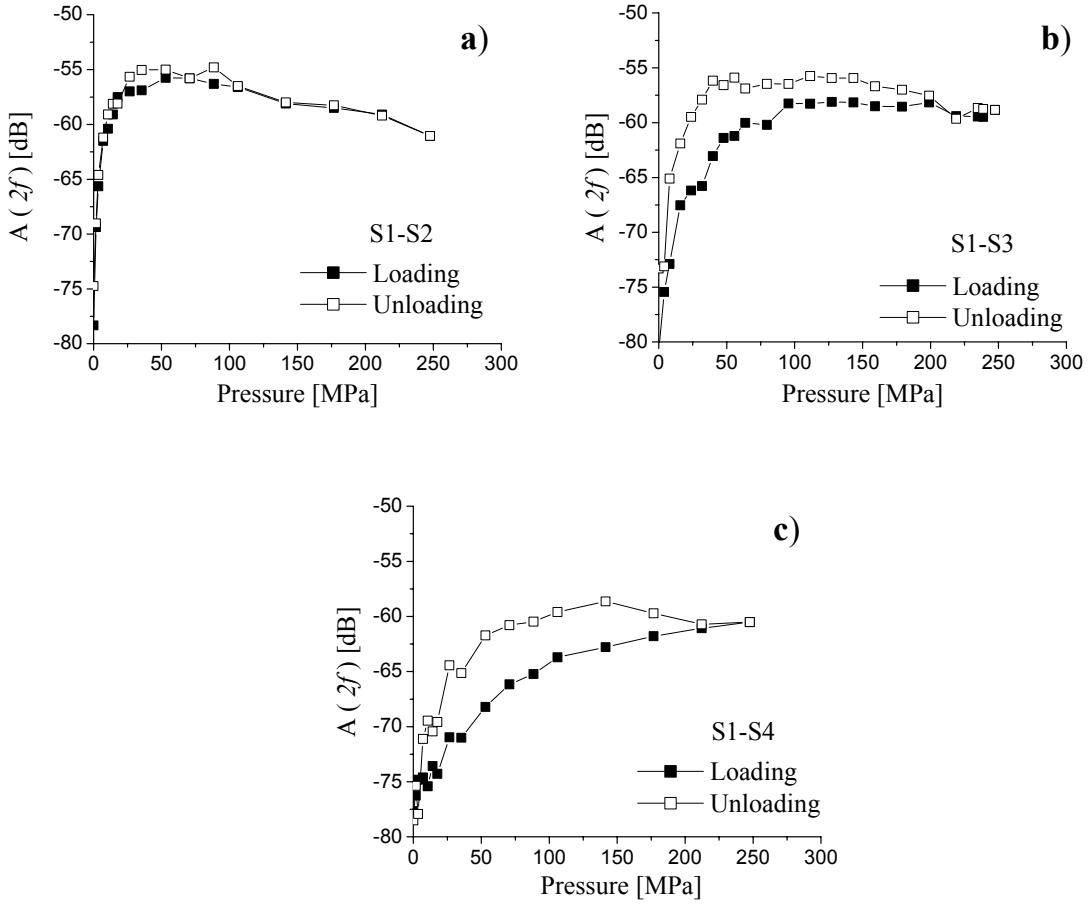

Figure 3. *Amplitude of the second harmonic component generated by the interface a) S1-S2, b) S1-S3, c) S1-S4 as function of the applied pressure. The data have been acquired during the loading and unloading phases of the same cycle.*

2.2 Water-confining Steel-Steel Interface

Measurements of the acoustic response of water-confining, rough surfaces in contact have been carried out using de-ionized water as the intermediate liquid layer between two rough surfaces. Water has been applied to the surface of the sample S1 in a quantity which assures that the whole extent of the interface is covered by the water layer once the second sample is placed onto S1. In the arrangement used here, water is not subjected to any lateral constraint outside that enforced by the two surfaces and their contacts. Thus,

outward (inward) drainage can occur when the applied pressure is increased (decreased). The sample combinations S1-S3 and S1-S4 have been utilized for these measurements. Figure 4a illustrates the linear response of these two interfaces as the applied pressure is increased from 0 to approximately 25 MPa. Note the initial dramatic reduction of the response of the smoother interface S1-S3, followed by a rather more gentle decrease with increasing pressure. A similar behavior characterizes also the response of the wet S1-S4 interface, although the initial negative variation is rather less pronounced. Figure 4b shows the dependence of the variation of the normalized interface stiffness of the two interfaces as a function of the applied pressure, the value of the stiffness when no pressure is applied reflecting the drop of the reflection coefficient due to the water layer alone. These plots also display rapid dramatic variations at pressure values below 5 MPa, which are not observed when the interface is dry. Therefore, a comparison between Fig. 2 and Fig. 4 suggests that some dramatic qualitative change occurs to the interface mechanics when water is trapped within the interface. In particular, note the nearly five-fold increase of the normalized stiffness value around 25 MPa due to the presence of water. As discussed next, a similar conclusion can be drawn from the measured values of the second harmonic amplitude versus the applied pressure as shown in Fig. 5.

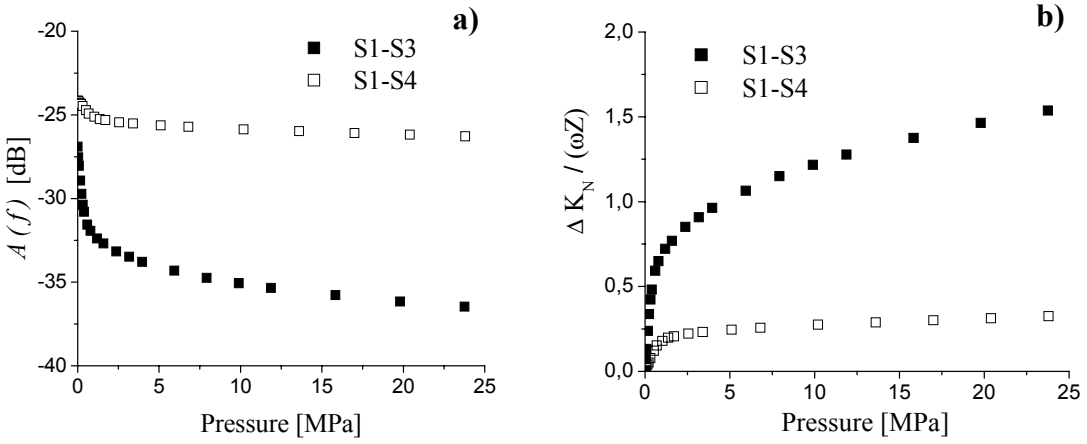

Figure 4. a) *Amplitude of the linearly reflected component by the water-confining interfaces S1-S3 and S1-S4 versus applied pressure; b) variation of the interface normalized stiffness versus applied pressure for the two interfaces considered in the previous figure. The data are acquired during loading.*

The measurements of the second harmonic generated by these two interfaces have been preceded by the assessment of the contribution of bulk water to the generation of the second harmonic. To this end, the area of the surface S1 which is insonified by the beam has been covered by a column of water with a thickness of about 20 mm. This value has been proven sufficient to avoid any interference between the signals reflected by the liquid-solid and liquid-air interfaces. The nonlinear response from the S1-water interface has been measured in the neighborhood of -73 dB, i.e. about 7 dB above the noise level due to the instrumentation used in this work. This result has been consistently obtained in several experiments.

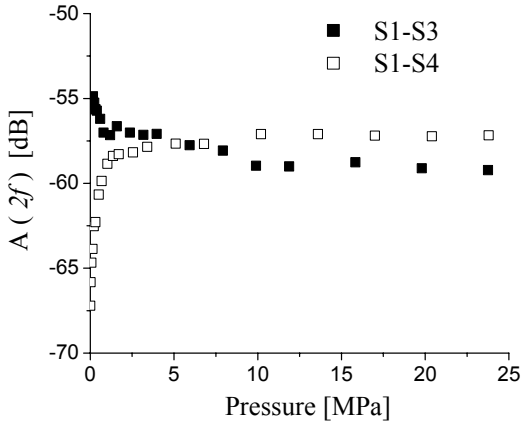

Figure 5. *Amplitude of the second harmonic component generated by the water-confining interfaces S1-S3 and S1-S4 versus applied pressure.*

Figure 5 illustrates the results obtained for the second harmonic generation by the two interfaces. In both cases, the values of the second harmonic amplitude at zero pressure is well above that of the bulk water, with that from the smooth interface larger by about 12 dB (-55.3 dB for S3 versus -67.2 dB for S4). Note also that the value of the initial opening configuration, which is expected to play an important role in the behavior of the interface at low loads, is a matter of educated guess. Finally, worthy of mention is the fact that, although the initial values of the modulus of $A(2f)$ reported above for the two interfaces may vary by a few decibels from test to test, a difference between them has been consistently observed.

For both interfaces, the modulus of $A(2f)$ reaches approximately the same maximum value within the pressure range considered here. Furthermore, unlike the linear response of the two interfaces, which presents strong qualitative similarities, their nonlinear responses display a marked difference. In fact, the response of the smoother interface steadily decays as the pressure increases while the response of the rough interface continues to increase, although at a rather low rate, for pressure values exceeding 2.5 MPa.

To summarize, the following has emerged from the results presented above:

i. the dependence of the amplitude of the wave reflected by a water-confining interface on the applied pressure is qualitatively rather different from that of a dry interface between the same surfaces,

ii. the dependence of the nonlinear response on the applied pressure varies dramatically with the surface topography,

iii. the maximum nonlinear response seems to be weakly dependent on the roughness of the interface,

iv. the bulk nonlinearity of water is not entirely responsible for that of the water-confining interfaces.

3. Discussion

3.1 Dry Steel-Steel Interfaces

The amplitude of the second harmonic wave generated by an elastic interface between two rough surfaces in contact and normalized by the amplitude of the incident wave, A_{in}, is given by (Pecorari 2003)

$$A(2f) = -\frac{\varepsilon}{4}\frac{jK_{N,0}^{*}}{1-jK_{N,0}^{*}}(T-1+R)^{2}. \qquad (1)$$

In eq. (1), $j=\sqrt{-1}$, $R=-1/(1-2jK_N^*)$ and $T=-2jK_N^*/(1-2jK_N^*)$ are the complex reflection and transmission coefficients of the fundamental wave, respectively. Note the combination $(T-1+R)$ which is proportional to the interface opening displacement

induced by the total stress field applied to the interface, and functions as excitation of the second harmonic components (Pecorari 2003). The symbol $\varepsilon = \left(K_{N,1}/K_{N,0}\right)A_{in}$ is a non-dimensional parameter which is much smaller than 1 in all the interface configurations of interest here. For a perfectly elastic interface, the quantities $K_{N,0}$ and $K_{N,1}$ are given by

$$K_{N,0} = n\left\langle \frac{E}{1-\nu^2} \right\rangle \left\langle \beta^{1/2} \right\rangle \int_0^{\delta_0} (\delta_0 - z)^{1/2} \varphi(z;N)\, dz\,, \tag{2}$$

and

$$K_{N,1} = \frac{n}{2}\left\langle \frac{E}{1-\nu^2} \right\rangle \left\langle \beta^{1/2} \right\rangle \int_0^{\delta_0} (\delta_0 - z)^{-1/2} \varphi(z;N)\, dz\,, \tag{3}$$

respectively. They are the first two coefficients of the series expansion of the interface stiffness, K_N, in powers of the variation of the interface relative approach, $\Delta\delta = -\Delta u$, where $\Delta u = A_{in}\left(T - 1 + R\right)$ is the interface opening displacement due to the total wave field:

$$K_N\left(\delta_0 + \Delta\delta\right) = K_{N,0} + K_{N,1}\Delta\delta = K_{N,0} - K_{N,1}\Delta u\,. \tag{4}$$

In eq. (2) and eq. (3), n is the number of contacts per unit area, E and ν are the Young modulus and the Poisson ratio of the material, respectively, and φ is the height distribution of the asperities of the composite surface, which, following Adler & Firman (1981), Brown & Scholz (1985), and Baltazar *et al*. (2002) is assumed to be a chi-square distribution. The composite surface is defined by a linear combination of the profiles of the two surfaces which maps the actual contacts of the interface onto the asperities of the composite surface. In addition to the composite height, z, φ depends on the parameter N ≥ 2, known as the *number of degrees of freedom*. For N = 2, φ is an exponential function, while for N→ ∞, it approaches a Gaussian distribution. The quantity δ_0 defines the approach between the mean planes of the two rough surfaces caused by the external load. It is null when no external pressure is acting on the interface. The symbol $\langle\cdots\rangle$ indicates the average over an ensemble of realizations of the composite interface. In eq. (2) and (3), β is the radius of curvature of the composite asperities, the distribution of which is assumed to be independent of z.

The result given in eq. (1) has been obtained by enforcing the nonlinear spring boundary conditions at the interface. The expressions for $K_{N,0}$ and $K_{N,1}$ are obtained from that linking the pressure, P, applied to the interface to the relative approach, δ, through successive derivations of the former with respect to the latter. This relationship assumes that the reaction of the interface to the applied pressure is the sum of those from each individual contact, and that each contact acts independently of the others according to Hertz law for two spheres in contact (Greenwood & Williamson, 1966).

The Hertz force law concerns itself with elastic contacts. In view of the experimentally observed behavior of the interfaces under examination, this law must be substituted with one which accounts for the elasto-plastic deformation of the asperities. Kim *et al.* have modified the model for surfaces in elastic contact and described the linear interaction of aluminum-aluminum elasto-plastic interfaces with an incident longitudinal wave, during a complete loading cycle. To that end they have adopted a new force law based on the finite-element analysis by Kogut & Etsion (2002) of an elasto-plastic sphere in contact with a rigid flat. This analysis accounts for the irreversible increase of the radius of curvature of the contact during loading. However, the behavior of each contact during the unloading phase of the cycle is assumed to be perfectly elastic, the radius of curvature of each contact remaining as it was at the end of the loading cycle (see Appendix A, eq. A8). An additional significant contribution of the model by Kim *et al.*, which is essential for a realistic description of the experimental results, is the realization that the dynamic interface stiffness at a given pressure during *loading* is that which the interface would display at the beginning of the *unloading* phase of the cycle, were the latter to start at this point. This element of the model is a generalization to an interface of a result by Johnson (1996) regarding a single contact.

A weak point of Kogut and Etsion's results is the discontinuity displayed by the force versus approach relationship at the transition between the elastic and the elasto-plastic regions. Jackson & Green (2005) have recently improved Kogut and Etsion's analysis providing an alternative empirical formulation of the force law, which is continuous over a range of values of the load reaching the fully plastic region (see Appendix A). Implementing this formulation of the force law for a single contact within the scheme devised by Kim *et al.*, the new relationship between P and δ is obtained, which, in

principle, should improve on that presented by Kim *et al*.. This relationship is still of the general form

$$P(\delta) = n\int_0^{\delta} F(z,\delta)\varphi(z;N)dz\ , \qquad (5)$$

where $F(z, \delta)$ is given in the Appendix both for loading and unloading. From this result, the coefficients $K_{N,0}$ and $K_{N,1}$ can be obtained by successive numerical differentiation, with the provision that during loading, the derivative is calculated as if unloading began at the particular point of the loading cycle under consideration. The linear and nonlinear responses of the interface are evaluated according to the well-known expression for the reflection and transmission coefficients reported above and to eq. (1), respectively.

Figure 6a-c presents a comparison between the experimental results of Fig. 2b and the theoretical predictions based on the model by Kim *et al*. modified by the use of Jackson and Green's force law. As in Kim *et al.*, the parameters of the model have been chosen as to provide a reasonable fit for the experimental results acquired during loading only (see Table II). In Table II, the parameter γ is related to the density of contact, *n*, by $n = \gamma/(\beta_o \sigma_c)$, where β_o represents the initial radius of curvature. Unlike in *Kim et al*., in this work the criterion employed to define the best choice was qualitative in nature and lacks objectivity and rigor. In other words, there may be other sets of parameters yielding theoretical curves fitting the experimental results equally well. Nonetheless, considering that the material parameters involved in the force law are common to the three interfaces, and those which determine the quality of the fit are related to the geometry of the individual contact and to the topography of the surfaces, this comparison offers a useful benchmark against which the current understanding of the effect of the latter set of parameters on the phenomena under investigation can be assessed.

The most remarkable feature of Fig. 6 is the progressive worsening with increasing roughness values of the fit between the data and the model results concerning the unloading phase of the cycle. This discrepancy is to be ascribed mostly to the inadequacy of the theoretical distribution of asperity height describing the topography of a plastically deformed interface, especially during unloading.

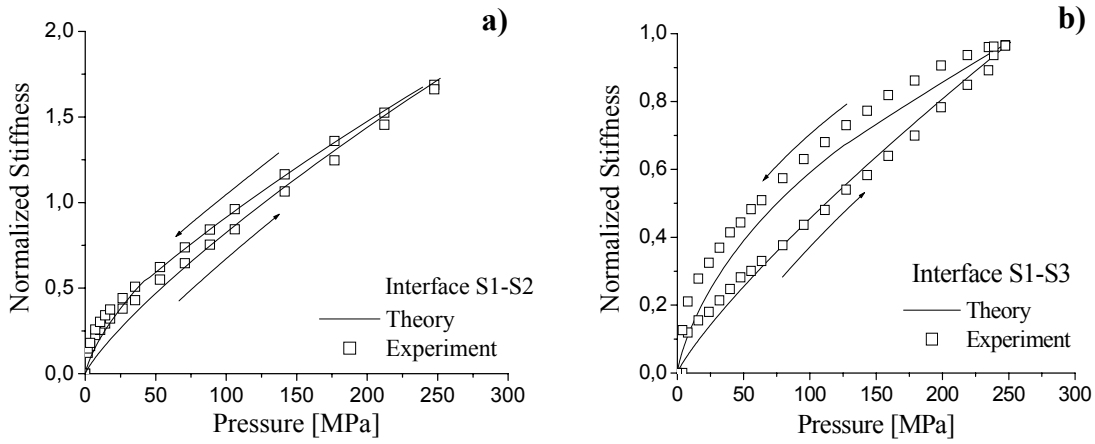

Figure 6. *Comparison between the experimental results and the theoretical predictions based on the fitting parameters presented in Table II. Linear reflection from the interface a) S1-S2, b) S1-S3, c) S1-S4.*

	N	γ (μm)	σ_c (μm)	S_Y (MPa)	β_o (10^4 μm)
S1-S2	16	4.8	0.38	270	$\sigma_c/3$
S1-S3	16	4.8	0.88	270	$\sigma_c/6$
S1-S4	12	4.8	1.68	270	$\sigma_c/6$

Table II. *Fitting parameters*.

In fact, the flattening of the highest asperities and the consequent variation of their height notwithstanding, the theoretical results for the unloading phase of the cycle are obtained by employing the distribution of the asperity height used during loading. In addition, after deformation the probability density of the radius of curvature of the asperities in contact can no longer be assumed to be independent of z, as it would be if the average value of the radius of curvature were to be used for all the contacts. An even more obvious drawback of the model is that the number of asperities involved in the integral relation between pressure and relative approach during loading and unloading are different, the former being larger than the latter. This is due to the need to exclude those contacts on which the force becomes negative during unloading at positive values of the approach from the integral of Eq. 5 (see Appendix A).

The comparison between the experimental and theoretical results concerning the linear response is not affected by the value of the amplitude of the incident wave, A_{in}. This is

not the case for the nonlinear response, given the linear dependence of the nonlinear parameter, ε, on A_{in}. Thus, when plotted in units of dB as in Fig 7, the contribution of A_{in} to the amplitude of the nonlinear response amounts to an additive constant. In view of this consideration, it follows that the comparison presented in Fig. 7a-c may address only the qualitative features of the data presented there, among which the following are worthy of attention.

The variation of the measured amplitude of the second harmonic with increasing (decreasing) stiffness during loading (unloading) is slower than that shown by the model predictions. This result lends further support to the development of nonlinear ultrasonic techniques to detect partially closed cracks, since it proves the persistence of a nonlinear response over a range of pressure values which is larger than that predicted theoretically.

A significant difference between the theoretical nonlinear response during loading and unloading is observed to occur at small values of the normalized stiffness. The experimental results, on the other hand, appear to display no significant hysteresis when plotted against the interface stiffness. In other words, according to the reported observations, the generation of the second harmonic measured in dB seems to be determined, apart from a constant proportional to the amplitude of the incident wave, entirely by the stiffness, that is to say, by an intrinsic property of the interface. This is also the case of the linear response. Therefore, in the specific cases of elastic and elasto-plastic dry interfaces, nonlinear acoustic measurements should not be expected to add information about the several mechanical and geometrical parameters determining the dynamics of the interface which is not already available via linear results. They may, however, provide an alternative and sometimes more convenient window through which a material may be inspected for partially closed surface-breaking cracks.

This feature may be attributed to the discontinuity of the derivative of the radius of curvature at the transition between the elastic and the elasto-plastic region during unloading. In fact, consistent with the expectation that smoother surfaces are less affected by plastic deformation than surfaces with high rms roughness, this variation occurs increasingly later during unloading as the surface roughness increases.

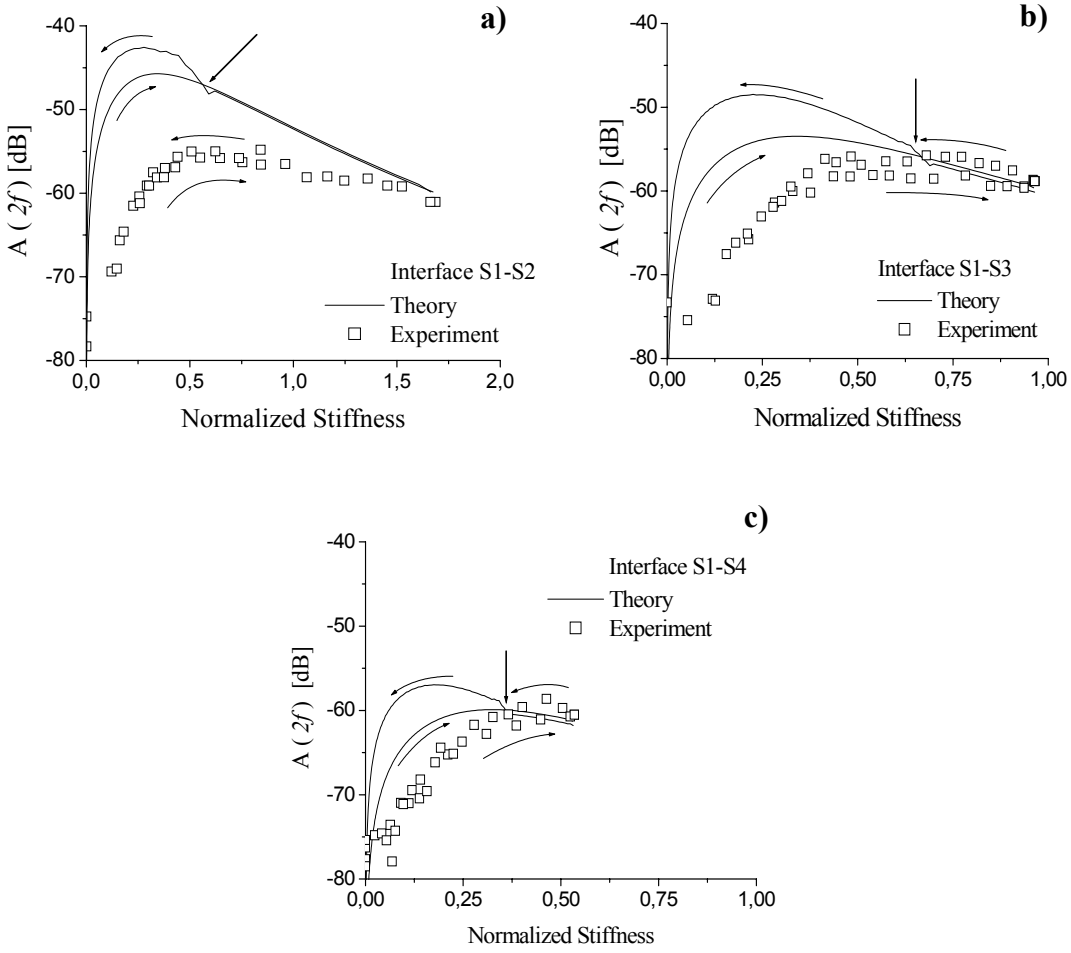

Figure 7. *Comparison between the experimental results and the theoretical predictions based on the fitting parameters presented in Table II. Second harmonic component generated by the interface a) S1-S2, b) S1-S3, c) S1-S4.*

In conclusion, the present state of the art in modeling the acoustic response of an elasto-plastic interface appears to be in need of a more realistic description of the topography of the surfaces in contact, and in particular, of the changes caused to it by successive loading cycles. A condition any newly proposed model must satisfy is the conservation of the number of asperities involved during a complete loading cycle. Furthermore, the variation of the radius of curvature during a cycle must occur in such a way that the continuity of its derivative with respect to the relative approach is respected.

3.2 Water-confining Steel-Steel Interface

Dwyer-Joyce *et al.* (2003) have investigated the feasibility of measuring the thickness of a thin liquid layer between two solid media by ultrasonic waves with a wavelength much larger than the layer thickness. By modeling the liquid as a layer of elastic springs with no thickness and stiffness $K_N = \Lambda/h$, where Λ is the known non-zero Lame' elastic constant of the liquid, and h is the unknown thickness of the layer, they estimate the value of K_N from the measured reflection coefficient of the layer, and from this h. This method is affected by some limitations linked to the sensitivity of the technique, which the authors duly discuss. This critique, however, does not prevent Dwyer-Joyce et al. from suggesting that the proposed technique allows values of the layer thickness of the order of 2 nm to be measured by using waves at a frequency of 60 MHz.

In the following, an additional limitation of this method is discussed, which concerns the ratio between the average distance between the solid surfaces and the rms roughness of the latter, and further specifies the conditions under which measuring a layer thickness of the order of a few nanometers with the proposed technique becomes feasible, at least in principle. When the variation of the interface profile is comparable with the average distance between the mean planes of the surfaces, there is no proven relationship currently available, either theoretical or experimental, between the value of the interface stiffness estimated by acoustic methods and the average distance between any couple of well-defined, nominally flat solid surfaces associated with the interface. Furthermore, at values of the average distance between the surfaces' mean planes of the order of, or smaller than, σ_c, mechanical contact between the surfaces occurs, and modeling the stiffness of the liquid layer as $K_N = \Lambda/h$ is no longer justified. From all this, and ignoring the effect of all the liquid-mediated forces which may act between two surfaces at distances below 100 nm (see the discussion below), it follows that thickness values of the order of a few nanometers can be measured by the proposed method only if the rms roughness of the limiting surfaces is of atomic scale.

The above remarks are relevant to the discussion of the results of Fig. 4, because, the mechanical contact between the surfaces having been established at macroscopic level in the reported experiments, the spring model employed by Dwyer-Joyce *et al.* alone no

longer suffices to account for the results presented here. Indeed, the sudden variations of the reflected wave's amplitude (Fig. 4a) and of the layer stiffness (Fig. 4b) before the applied pressure reaches 5 MPa cannot be reproduced even by a model which combines the stiffness of the thin fluid layer model, $K_N = \Lambda/h$, with that of the dry contacts. Additional physical elements are needed (Pecorari 2005).

Thanks to the advent of the surface force apparatus (SFA) and of the atomic force microscope (AFM) with its several variants, the interaction between solid surfaces in presence of a liquid has been extensively studied over the last twenty years. In these investigations, surfaces with planar, cylindrical or spherical geometry, roughness of atomic size, and well-defined chemical composition are routinely employed. A thorough survey of this body of knowledge can certainly provide enough material for a book, and obviously goes beyond the scope of this communication and of its authors' competence. However, of the several types of force which may contribute to the interaction between two solid surfaces separated by a thin layer of liquid (Israelashvili 1992), two display the repulsive character and intensity which make them compatible with the observed data. The first type of force, known as "double layer" force, appears when ions are exchanged between an electrolytic solution and the solid surfaces. The excess charge distributed over the solid surfaces attracts others of the opposite sign from the solution and, together, form double layer structure. As two surfaces approach, the double layer structure associated with each surface tends to repel the other with a force having a range of action which may vary between 10 nm and 100 nm. The second class comprises forces which are also highly repulsive and are felt at most over distances of the order of a nanometer. The origin of these forces is less understood, and apparently not unique. They may appear exclusively because of the increased spatial order of the fluid molecules arising when the latter are confined within a volume with dimensions comparable with their diameter. The increased structural order leads to additional external work being required to remove the few remaining layers of the fluid before the mechanical contact between two surfaces can be established. Given their origin, these forces are known as "structural" forces. The increase in the fluid's structural order can be facilitated also by the electrical field generated by ions which have been absorbed onto the solid surface from the solution. These repulsive forces are known as "hydration" or "solvation" forces,

depending on whether the solvent is water or else. Hydration and solvation forces may also display an oscillatory behavior which follows the solid-like layered structure of a liquid in confinement (Pashley & Israelachvili 1984, Israelachvili 1992, Leikin & Kornyshev, 1990). Das et al., 1996 have evaluated the intensity of these forces in the range between 1 and 100 MPa for distances between the surfaces of the order of a few molecular diameters. Of interest also is the observation by Grabbe and Horn (1993) who noted that a pressure between 1 and 10 MPa must be exerted onto the two surfaces of an SFA in order to achieve contact between them. Considering their repulsive nature and intensity at short distance, this type of force is a prime candidate to explain the effects reported in this work. This interpretation is also supported by additional experiments not reported here on systems in which water has been substituted by lubricating oil. Even in this case, a sharp decrease of the linearly reflected wave like that shown in Fig. 4 is observed as the applied pressure is increased after the formation of the first contacts. Indeed, in view of the considerable difference between the electric and structural properties of water and lubricating oil, as well as the consistency of the experimental observations with steel surfaces regardless their state of oxidation, the evidence gathered so far suggests that this strong repulsive force is mainly of the "structural" type.

At the end of this discussion, only a brief mention is reserved for the great wealth of research on the molecular structure of water in close proximity to liquid/solid interfaces. The role of directional features of the hydrogen bond and of the hydrophobic or hydrophilic character of the substrate has been shown to be at the root of several important properties of interfacial water at mesoscopic scale, and, in particular, of a phase transition between the bulk structure of the liquid and one which is typical of its solid phase. (Heuberger *et al.*, 2002 and references therein, Ruan *et al*., 2004, Scatena *et al.*, 2002, Soper & Ricci, 2001). Although estimates of the effects of these phenomena on the elastic properties of the liquid confined by the solid surfaces are still to come, and the relationship between the structure of molecular water and the forces by which two surfaces may interact is not yet well explored, the relevance of this subject to the observations presented here cannot be overestimated.

To the present day, the interaction between low frequency ultrasonic waves and liquid-confining, rough surfaces at distances below 100 nm from each other is still poorly

understood. It is these authors' opinion that progress in this area necessitates the development of models which duly account to for the physics of liquids in confinement. The considerable amount of information gathered on liquid-mediated forces between solid surfaces by means of AFM and SFA offers a solid starting point for this effort.

A deeper understanding of the acoustic fingerprint of liquid-mediated forces between solid surfaces in environments commonly found in industrial settings may lead to significant technological advances. Of these, noninvasive techniques to monitor the condition of lubricating films in industrial machinery, or the evolution of chemical and physical processes affecting liquids in confinement, are two important examples. In other words, besides the satisfaction of academic curiosity, the motivation for understanding the interaction between acoustic waves and liquids in confinement is rooted in the potential development of more efficient and intelligent production processes.

Conclusions

This communication reports experimental results which lead to the conclusion that the theoretical models currently available to describe the macroscopic properties of dry elasto-plastic surfaces in contact are still defective. In particular, the statistical distribution of the asperities in contact has been identified as a key element of the model in need of substantial revision. When plotted against the interfacial stiffness, both linear and nonlinear scattering properties appear to be completely determined by the normalized interfacial stiffness. Thus, they should be regarded as equivalent tools to characterize partially closed elasto-plastic interfaces, offering two alternative ways to inspect material components. Finally, the experimental results presented here may be considered as a step forward in the continuous development of inspection techniques for the detection of dry and partially closed cracks.

As for the acoustic response of liquid-confining rough surfaces in contact, or at distances less than 100 nm, the results obtained with steel surfaces entrapping de-ionized water show how the latter greatly enhances the nonlinear response of a crack which is nearly open. These findings suggest that inspection techniques exploiting the nonlinear properties of partially closed cracks may be employed to detect these defects even when

they are nearly open provided they are fluid-filled. Moreover, they indicate that simplistic models accounting only for the bulk properties of the liquid are inadequate for the purpose of predicting the acoustic response of such interfaces. In fact, granted the need for additional and broader experimental evidence on the phenomena investigated in this work, the available evidence documenting the relevance of liquid-mediated forces between solid surfaces and the results reported here suggest that highly repulsive, short range forces due to the increased order of the confined liquid structure may be the cause of the observed dramatic interface stiffening. This interpretation of the experimental results is also supported by a theoretical model (Pecorari 2005).

Acknowledgements

This work was partially supported by the Swedish Inspectorate for Nuclear Power, (contract # 14.43-010902,01156), by the Swedish Centre for Nuclear Technology (project title: "Detection of SCCs by means of nonlinear scattering of ultrasonic waves"), and by the Swedish Research Council (contract # 621-2003-4320). The NATEMIS program supported by European Science Foundation has provided the framework for valuable discussions between of one the authors (C. P.) and the group of Dr. W. Arnold at the IZFP in Saarbrücken (Germany). Finally, the authors would like to thank Dr. S.I. Rokhlin for bringing to their attention the work by Jackson and Green and for his support and encouragement.

Appendix A

According to the model developed by Jackson and Green (2005), the FEM results on the force versus distance law for a hemispherical contact during approach can be approximated by the following empirical formulation. Let

$$h_c = \left(\frac{\pi C S_y}{2E'} \right)^2 \beta \qquad \text{(A.1)}$$

be the approach after contact at which the interaction is not longer purely elastic. In eq. A.1, C = 1.295 exp(0.736 ν), where ν is the Poisson ratio of the material, S_y is the yield strength, $1/E' = \left(1 - v_1^2\right)/E_1 + \left(1 - v_2^2\right)/E_2$, where the subscripts 1 and 2 refer to the two

spheres in contact, and $1/\beta = 1/\beta_1 + 1/\beta_2$, where β_i is the radius of curvature of the *i*-th sphere. By introducing the expression for the critical approach in the Hertz law for elastic spheres in contact, the critical force marking the onset of plasticity is obtained

$$F_c = \frac{4}{3}\left(\frac{\beta}{E'}\right)^2 \left(\frac{C}{2}\pi S_y\right)^3 . \qquad \text{(A.2)}$$

By defining the normalized relative approach, $\overline{h} = h/h_c$, the normalized applied force, $\overline{F} = F/F_c$, can be written as follows:

$$\overline{F} = \overline{h}^{3/2}, \qquad \text{for } 0 \le \overline{h} \le \overline{h}_t \qquad \text{(A.3)}$$

and

$$\overline{F} = \left[\exp\left(-\frac{1}{4}\left(\overline{h}\right)^{5/12}\right)\right]\overline{h}^{3/2} + \frac{4H_G}{CS_y}\left[1-\exp\left(-\frac{1}{25}\left(\overline{h}\right)^{5/9}\right)\right]\overline{h}, \quad \text{for } \overline{h} > \overline{h}_t . \qquad \text{(A.4)}$$

The quantity $\overline{h}_t = 1.9$. In eq. A.4, H_G is the hardness geometric limit, and the ratio H_G/S_y is given by

$$\frac{H_G}{S_y} = 2.84\left[1-\exp\left(-0.82\left(\frac{\pi C e_y}{2}\overline{h}\left(\frac{\overline{h}}{\overline{h}_t}\right)^{B/2}\right)^{-0.7}\right)\right], \qquad \text{(A.5)}$$

where $e_y = S_y/E'$, and $B = 0.14\exp(23e_y)$. During loading the normalized area of contact, $\overline{A} = A/A_c$, where $A_c = \pi^3\left(CS_y\beta/2E'\right)^2$, varies as

$$\overline{A} = \overline{h}\ , \qquad \text{for } 0 \le \overline{h} \le \overline{h}_t , \qquad \text{(A.6)}$$

and

$$\overline{A} = \overline{h}\left(\frac{\overline{h}}{\overline{h}_t}\right)^B , \qquad \text{for } \overline{h} > \overline{h}_t . \qquad \text{(A.7)}$$

During unloading, the force versus approach relationship is assumed to be perfectly elastic, and described by the following relationship (Li *et al*., 2002)

$$\overline{F} = \overline{F}_{\max} - \sqrt{\frac{\beta_{\max}}{\beta_o}}\left[\overline{h}_{\max}^{3/2} - \overline{h}^{3/2}\right], \qquad \text{(A.8)}$$

where $\beta_{\max}$ and $\overline{h}_{\max}$ are the maximum radius of curvature and normalized approach reached during loading. The symbol β_o represents the initial value of the radius of curvature. The radius of curvature, β, which during unloading maintains its maximum value $\beta_{\max}$, is related to the approach and radius of the area of contact by $\beta = a^2/h$, and a is obtained from $A = \pi a^2$. Finally, note that $\overline{F}$ becomes negative for positive values of the approach $\overline{h}$ which are smaller than $\overline{h}^* = \left[\overline{h}_{\max} - \overline{F}_{\max}\sqrt{\beta_o/\beta_{\max}}\right]^{2/3}$. Thus, during unloading the asperities contributing to the total pressure with unphysical negative values of the force $\overline{F}$ must be excluded from the integration.

References

Adler, R.F. & Firman, D. 1981 A non-Gaussian model for random surfaces. *Philos. Trans. Roy. Soc. London A* **303**, 433-462.

Baltazar, A., Rokhlin, S.I. & Pecorari, C. 2002 On the relationship between ultrasonic and micromechanic properties of contacting rough surfaces. J. of Mech. Phys. Solids **50**, 1397-1416.

Biwa, S., Nakajima, S., & Ohno, N. 2004 On the acoustic nonlinearity of solid-solid contact with pressure-dependent interface stiffness. *J. Appl. Mech.* **71**, 508-515.

Brown, S.R. & Scholz, C.F. 1985 Closure of random elastic surfaces in contact. *J. Geophys. Res.* **90**, 5531-5545.

Das S.K., Sharma M.M. & Schechter R.S. 1996 Solvation force in confined molecular fluids using molecular dynamic simulation. *J. Phys. Chem*. **100**, 7122-7129.

Drinkwater, B.W., Dwyer-Joyce, R.S. & Cawley P. 1996 A study of the interaction between ultrasound and partially contacting solid-solid interface. *Proc. Roy. Soc. Lond. A* **452**, 2613-2628.

Dwyer-Joyce, R.S., Drinkwater, B.W. & Donohoe, C.J. 2003 The measurement of lubricant-film thickness by ultrasound. *Proc. Roy. Soc. Lond. A* **459**, 957-976.

Grabbe A. & Horn R.G. 1993 Double-layer and hydration forces measured between silica sheets subjected to various surface treatments. *J. Coll. Interf. Sc*. **157**, 375-383.

Greenwood, J.A. & Williamson, J.B.P. 1966 Contact of nominally rough surfaces. *Proc. R. Soc. London A* **295**, 300-319.

Heuberger, M., Zäch, M. & Spencer, N.D. 2001 Density fluctuation under confinement: When is a fluid not a fluid? *Science* **292**, 905-908.

Kim, J.-Y., Baltazar A. & Rokhlin, S.I. 2004 Ultrasonic assessment of rough surface contact between solids from elastoplastic loading-unloading hysteresis cycle. *J. of Mech. Phys. Solids* **52**, 1911-1934.

Kogut, L. & Etsion, I. 2002 Elasticed-plastic contact analysis of a sphere and a rigid flat. *J. Appl. Mech.* **69**, 657-662.

Israelachvili, J.N. 1992 *Intermolecular and surface forces*, 2nd edn. Academic Press, London, 213-312.

Jackson, R. L. & Green, I. 2005 A finite element study of elasto-plastic hemispherical contact. *J. of Tribology* **127**, 343-354.

Johnson, K.L. 1996 Modeling the indentation hardness of solids. *Proceedings of the First Royal Society-Unilever Indo-UK Forum in Material Science and Engineering*, *Solid-Solid Interaction.* Imperial College Press, London, 16-28.

Leikin, S. & Kornyshev, A.A. 1990 Theory of hydration forces. Nonlocal electrostatic interaction of neutral surfaces, *J. Chem. Phys.* **92**, 6890-6898.

Li, L-Y., Wu, C-Y & Thornton, C. 2002 A theoretical model for the contact of elastoplastic bodies. *Proc. Instn. Mech. Engrs.* **216** (Part C), 421-431.

Pashley, R.M. & Israelashvili, J.N. 1984 Molecular layering of water in thin films between mica surfaces and its relation to hydration forces. *J. Colloid and Interface Science* 101, 511-523.

Pecorari, C. 2003 Nonlinear interaction of plane ultrasonic waves with an interface between rough surfaces in contact. *J. Acoust. Soc. Am.* **113**, 3065-3072, and references therein.

Pecorari, C. 2004 Adhesion and nonlinear scattering by rough surfaces in contact: Beyond the phenomenology of the Presach-Mayergoyz framework. *J. Acoust. Soc. Am.* **116**, 1938-1947.

Pecorari, C. & Poznic, M. 2005 Nonlinear acoustic scattering by a partially closed surface-breaking crack. *J. Acoust. Soc. Am.* 117, 592-600.

Pecorari, C. 2005 Structural forces and the acoustic properties of liquid-confining interfaces. *To be submitted for publication*.

Ruan, C-Y., Lobastov, V.A., Vigliotti, F., Chen, S. & Zewail, A. 2004 Ultrafast electron crystallography of interfacial water. *Science* **304**, 80-84.

Scatena, L.F., Brown, M.G. & Richmond, G.L. 2001 Water at hydrophobic surfaces: Weak hydrogen bonding and strong orientation effects. *Science* **292**, 908-912.

Soper, A.K., & Ricci, M.A., 2001 Structure of high-density and low-density water, *Phys. Rev. Lett.* **84**, 2881-2884.

PAPER B

Nonlinear acoustic scattering by a partially closed surface-breaking crack

Claudio Pecorari and Milan Poznić
Marcus Wallenberg Laboratory, Royal Institute of Technology, 100 44 Stockholm, Sweden

(Received 23 April 2004; revised 22 November 2004; accepted 25 November 2004)

A theoretical model describing the nonlinear scattering of acoustic waves by surface-breaking cracks with faces in partial contact is presented. The nonlinear properties of the crack are accounted for by suitable boundary conditions that are derived from micromechanical models of the dynamics of elastic rough surfaces in contact. Both linear and nonlinear responses of the crack are shown to be largest for a shear vertical wave incident on the surface containing the crack at an angle just above the critical angle for longitudinal waves. These findings question the fitness for the purpose of a conventional inspection method, which utilizes shear vertical waves at 45° of incidence to search for surface-breaking cracks in many engineering components. For angles of incidence proximal to the critical angle of longitudinal waves, the efficiency of the second harmonic's generation appears to be the highest. Thanks to the increased sensitivity to surface-breaking cracks, this configuration seems to offer a solution to the localization problem, a task that has eluded nonlinear techniques operating under other circumstances. Finally, this model suggests a simple interpretation of the highly localized nonlinear response of delaminations in composite materials.
 [DOI: 10.1121/1.1850052]

PACS numbers: 43.25.Dc, 43.25.Jh, 43.25.Ts, 43.35.Zc [MFH] Pages: 592–600

I. INTRODUCTION

Material components containing cracks respond to an external dynamic perturbation in a nonlinear manner.[1,2] For instance, when insonified by a harmonic wave, the spectrum of the acoustic response of a cracked sample has been shown to display higher-order harmonic components, which are not found in samples without cracks. Similarly, if a component containing a partially closed crack is tested simultaneously by two harmonic waves of frequencies f_1 and f_2, with $f_1 \gg f_2$, signals are generated within the sample, which contain sideband components at frequencies $f_1 \pm f_2$. These, again, are not found in the acoustic fields generated by scattering events in material components without cracks.

An even richer phenomenology[3] can be observed when the amplitude of the excitation is increased beyond the threshold value at which clapping between the crack's faces is activated. For example, the generation of subharmonic components, which is the first step toward a chaotic regime of vibration, can be observed by progressively increasing the excitation amplitude. Nonlinear effects caused by the dissipation of the acoustic energy have also been reported in experiments conducted on cracked glass samples.[4,5]

The experiments mentioned above are often performed with continuous waves at frequencies that are well below the MHz range, so that the wavelength of the waves propagating within the inspected component is of the order of several centimeters. As the whole volume of the material is insonified, and the acoustic response is commonly detected by using a stationary sensor, the localization of the defect under such experimental conditions is a very difficult task.

An important variation of this approach is that developed by Krohn *et al.*[6] in which the local response of a composite plate to a low-frequency, large-amplitude acoustic wave source is detected by a scanning laser interferometer. In these experiments, the plate's thickness is much smaller than the wavelength of the probing acoustic wave. The large values of the wave amplitude utilized in these experiments suggest that the mechanism responsible for the nonlinear response of the plate is clapping between the faces of the delamination. This hypothesis is further supported by the presence of harmonics of very high order in the scattered acoustic field. Images of the plate formed by displaying the amplitude variation of higher-order harmonics, or other nonlinear components, show a feature of great importance for practical applications: the highly localized nonlinear response of the defect, which decays by as many as 20 dB as the observation point moves away from the defect. A convincing explanation of such an interesting phenomenon has yet to be provided.

A few authors have developed models that predict the nonlinear response of cracks with faces interacting with each other. Achenbach and Norris[7] have analyzed the effect of clapping on the linear response of a crack insonified by an incident wave. Boundary conditions along the crack's faces, which require the continuity of the total displacement when the crack is closed, and set the total applied stress to zero when the crack is open, have been used. Hirose and Achenbach[8] have developed a sophisticated mathematical approach to modeling nonlinear scattering by a circular crack with clapping faces. The time evolution of the clapping faces is followed by numerically solving an appropriate integral equation, the solution of which is used to evaluate the scattered field in the space–time domain. The harmonic content of the scattered field is recovered via a Fourier analysis of the latter. A similar approach has also been adopted by Hirose,[9] who employs more realistic boundary conditions at the crack's face. In fact, Hirose considers the interaction between the crack's faces to occur only at discrete locations

and at instants that are determined by the time evolution of the applied load, by the crack's initial conditions, and by the topography of the two surfaces. Donskoy, Sutin, and Ekimov[10] have proposed a simplified mathematical scheme to account for the effect of the nonlinearity introduced by Hertzian contacts between the crack surfaces that are assumed to be rough and nonconforming. To this end, they have used the spring model[11] for imperfect interfaces to formulate the nonlinear boundary conditions at the surface of the crack. Thus, the dynamics of a collection of contacts is simulated by that of two distributions of nonlinear springs having normal and tangential stiffness constants, K_N and K_T, respectively. Donskoy *et al.*, however, have considered only the effect of the normal mode of vibration on the nonlinear scattering process.

While all the theoretical work cited above concerns itself with cracks that are imbedded into the bulk of the hosting material component, in this investigation the focus is on the acoustic response of surface-breaking cracks, of which stress-corrosion cracks are typical and extremely important examples. The mathematical description of the problem at hand is provided by an extension of a previous model[12] dealing with the linear wave scattering by surface-breaking cracks with faces in partial contact to include the generation of the second harmonic component. As in the work of Donskoy *et al.*, the spring model for imperfect interfaces is employed to incorporate the nonlinear properties of the crack into the boundary conditions enforced on the total scattering field along the crack faces. In this investigation, however, the nonlinear dynamics of rough surfaces in contact is described in terms of a more recent approach.[13] The latter yields the nonlinear dependence of both spring constants, K_N and K_T, on the local relative approach between the crack's faces. A closer examination shows that both the force law governing the interaction between asperities in contact and the surface topography play a key role in determining such dependence. The nonlinear scattering problem is solved by using a standard perturbation technique, the small perturbation parameter naturally arising from the normalization of the boundary conditions as a measure of the system's nonlinearity. The dependence of the scattered second harmonic on the type of incident wave, on the interface spring constants, on the crack depth, and on the spatial coordinates of the observation point is investigated. The spatial evolution of the linear and nonlinear components of the scattered field is also evaluated up to distances of the order of ten wavelengths of the incident wave from the crack. A discussion of the relevance of these results on the nondestructive inspection of components containing surface-breaking cracks concludes this work.

As a final remark, it is stressed that the purpose of the model developed in this work is limited to the following: (i) providing general guidance to optimize the configuration of the inspection system to detect shallow surface-breaking cracks; and (ii) aiding physical intuition in the interpretation of experimental results with respect to the role played by the relevant physical and geometrical parameters of the system. No claim is made as to the potential use of this model to accurately predict the acoustic response of real cracks in hosting materials with a complex microstructure. The number of parameters determining the acoustic response of a real crack under such circumstances is too large, and our knowledge of their values is so poor that the goal of providing accurate theoretical predictions of acoustic scattering experiments carried out in real life situations is simply unattainable at the present time and, perhaps, will remain so for some time.

II. THEORY

A complete set of boundary conditions to be enforced on the total acoustic field at an interface between two rough surfaces in contact has been derived by Pecorari[13] under the assumption that the interaction between the asperities is purely elastic. If the interface is assumed to coincide with the plane of equation $x_1=0$, the boundary conditions are

$$\frac{1}{2}(\sigma_{31}^{+}+\sigma_{31}^{-})=K_{T,0}\,\Delta\nu-K_{T,N}\,\Delta u\,\Delta\nu-\frac{1}{2}K_{T,1}\Bigg[(\Delta\nu^2-\Delta\nu_{\max}^2)\operatorname{sgn}\left(\frac{\partial\Delta\nu}{\partial t}\right)+\Delta\nu\,\Delta\nu_{\max}\Bigg], \quad (1a)$$

$$\frac{1}{2}(\sigma_{11}^{+}+\sigma_{11}^{-})=K_{N,0}\,\Delta u-K_{N,1}\,\Delta u^2, \quad (1b)$$

$$\sigma_{31}^{+}=\sigma_{31}^{-}, \quad (1c)$$

$$\sigma_{11}^{+}=\sigma_{11}^{-}. \quad (1d)$$

In Eqs. (1a)–(1d), u and ν are the components of the total displacement in the x_1 and x_3 directions, respectively, $\Delta u=(u^{+}-u^{-})$ and $\Delta\nu=(\nu^{+}-\nu^{-})$ are the corresponding interface opening displacements, and $\sigma_{ij}^{+,-}$, with $i, j=1, 3$, is the ijth stress component of the stress field acting on the interface. The superscript $+(-)$ refers to the half-spaces for which x_1 is positive (negative). All the field quantities are to be understood to be functions of time, t. The coefficients K's are derived from suitable micromechanics models, which assume the elastic normal and tangential interaction between asperities to be described by the Hertz[14] and Mindlin and Deresiewicz[15] models, respectively, of two elastic spheres in contact. In particular, $K_{N,0}$ and $K_{T,0}$ can be found to be[13]

$$K_{N,0}=n\left\langle\frac{E}{1-\nu^2}\right\rangle\langle\beta^{1/2}\rangle\int_0^{\delta_0}(\delta_0-z)^{1/2}\varphi(z)dz, \quad (2)$$

and

$$K_{T,0}=2n\left\langle\frac{E}{(1+\nu)(2-\nu)}\right\rangle\langle\beta^{1/2}\rangle\int_0^{\delta_0}(\delta_0-z)^{1/2}\varphi(z)dz. \quad (3)$$

In Eqs. (2) and (3), n is the number of contacts per unit area, E and ν are the Young modulus and the Poisson ratio of the material, respectively, β is the radius of curvature of the asperities, and φ is the height distribution of the asperities of the composite surface. The latter is defined by a linear combination of the profiles of the two surfaces, which maps the actual contacts of the interface onto the asperities of the composite surface.[13] The quantity δ_0 defines the approach between the mean planes of the two rough surfaces caused by the external load, and it is null when no external pressure is

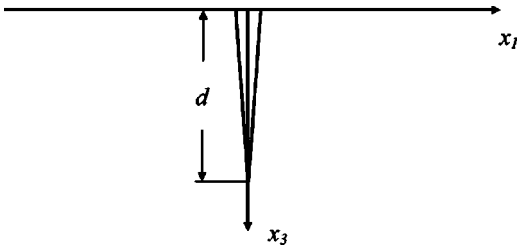

FIG. 1. Schematic representation of the surface-breaking crack and of the coordinate systems used in the model.

acting on the interface. The symbol $\langle \cdots \rangle$ indicates a statistical average. Thus, $K_{N,0}$ and $K_{T,0}$ can be evaluated numerically in terms of the mechanical and topographic properties of the two rough surfaces in contact. The magnitude of K_N and K_T varies with the load applied to the interface, and so does the ratio K_T/K_N, which, however, remains of the order of 0.5. Similar expressions can be found for $K_{N,1}$, $K_{T,1}$, and $K_{N,T}$. The reader who is interested in further details is referred to the original paper.[13]

To the first order of approximation, the nonlinear effect due to the hysteretic component of the tangential stiffness is shown to be responsible for the generation of higher harmonics of odd order, the magnitude of which is considerably smaller than that of the second harmonic generated by the nonlinearity due to K_N. For this reason, in Eq. (1a) those terms that are linked to the latter mechanism can be neglected to obtain the following simplified version of nonlinear boundary conditions:

$$\frac{1}{2}(\sigma_{31}^{+}+\sigma_{31}^{-})=K_{T,0}\,\Delta\nu-K_{T,N}\,\Delta u\,\Delta\nu, \tag{4a}$$

$$\frac{1}{2}(\sigma_{11}^{+}+\sigma_{11}^{-})=K_{N,0}\,\Delta u-K_{N,1}\,\Delta u^2, \tag{4b}$$

$$\sigma_{31}^{+}=\sigma_{31}^{-}, \tag{4c}$$

$$\sigma_{11}^{+}=\sigma_{11}^{-}. \tag{4d}$$

Equations (4a) and (4b) describe an imperfect interface, the stiffness constants of which increase when the surfaces in partial contact approach each other. Furthermore, since the spring model for an imperfect interface is an effective approach to describing the interface properties, and the latter are assumed constant along the interface, the term ''partial contact'' is to be understood as referring to the discontinuity of the contact that occurs at a microscopic level.

The mathematical formulation of the problem in which an incident wave is scattered by a surface-breaking crack with nonlinear boundary conditions is presented next. The crack is assumed to be positioned on the positive semiplane of equation $x_1=0$, with its mouth placed at the origin of the coordinate system, while its tip reaches a depth d below the surface of the medium. The latter occupies the half-space defined by $x_3\geqslant 0$ (see Fig. 1).

Following the approach by Achenbach *et al.*[16] and Mendelsohn *et al.*,[17] the original problem is decomposed into a symmetric and an antisymmetric part, which are solved in the quarter-space $x_1\geqslant 0$, $x_3\geqslant 0$. The boundary conditions associated with these problems are as follows: *symmetric problem*,

$$\sigma_{13}^{+}=0, \quad x_1=0, \quad 0\leqslant x_3<\infty, \tag{5a}$$

$$\sigma_{11}^{+}=K_{N,0}\,\Delta u-K_{N,1}\,\Delta u^2, \quad 0\leqslant x_3<d, \tag{5b}$$

$$u=0, \quad d\leqslant x_3<\infty; \tag{5c}$$

antisymmetric problem,

$$\sigma_{11}^{+}=0, \quad x_1=0, \quad 0\leqslant x_3<\infty, \tag{6a}$$

$$\sigma_{13}^{+}=K_{T,0}\,\Delta\nu-K_{T,N}\,\Delta u\,\Delta\nu, \quad 0\leqslant x_3<d, \tag{6b}$$

$$\nu=0, \quad d\leqslant x_3<\infty. \tag{6c}$$

In Eq. (5b) and Eq. (6b), σ_{ij}^{+} are the components of the total stress field on the side of the crack facing the quarter-space for which $x_1>0$. They include the contribution of the incident wave. In both problems, the components σ_{33} and σ_{31} of the total stress field must be null at the surface $x_3=0$. Note that, in view of the continuity of σ_{11} and σ_{31} across the contacting surfaces of the crack as given by Eqs. (4c) and (4d), Eq. (5b) and Eq. (6b) can be formulated only in terms of the total stress components on the positive face of the crack.

Since the material half-space supporting the propagation of the acoustic waves is linear, the same equations of motion used by Achenbach *et al.*[16] and Mendelsohn *et al.*[17] apply,

$$c_L^2\frac{\partial^2 u}{\partial x_1^2}+c_T^2\frac{\partial^2 u}{\partial x_3^2}+(c_L^2-c_T^2)\frac{\partial^2 \nu}{\partial x_1\,\partial x_3}=\frac{\partial^2 u}{\partial t^2}, \tag{7}$$

$$c_L^2\frac{\partial^2 \nu}{\partial x_1^2}+c_T^2\frac{\partial^2 \nu}{\partial x_3^2}+(c_L^2-c_T^2)\frac{\partial^2 u}{\partial x_1\,\partial x_3}=\frac{\partial^2 \nu}{\partial t^2}. \tag{8}$$

In Eq. (7) and Eq. (8), c_L and c_T are the phase velocities of longitudinal and shear waves, respectively.

It is convenient to formulate the problem in nondimensional form. To this end, the displacement components are normalized with respect to the amplitude of the incident wave, A_{in}: $U=u/A_{\mathrm{in}}$, $V=\nu/A_{\mathrm{in}}$; the coordinates are rescaled with respect to the wave number of the longitudinal wave, k_L: $x_i=X_i/k_L$, and time is normalized by ω: $t=\tau/\omega$. Then, Eq. (7) and Eq. (8) become

$$\frac{\partial^2 U}{\partial X_1^2}+\frac{1}{\kappa^2}\frac{\partial^2 U}{\partial X_3^2}+\left(1-\frac{1}{\kappa^2}\right)\frac{\partial^2 V}{\partial X_1\,\partial X_3}=\frac{\partial^2 U}{\partial \tau^2}, \tag{9}$$

$$\frac{\partial^2 V}{\partial X_1^2}+\frac{1}{\kappa^2}\frac{\partial^2 V}{\partial X_3^2}+\left(1-\frac{1}{\kappa^2}\right)\frac{\partial^2 U}{\partial X_1\,\partial X_3}=\frac{\partial^2 V}{\partial \tau^2}, \tag{10}$$

in which $\kappa=c_L/c_T$.

The boundary conditions are also similarly transformed, and, in particular, Eq. (5b) and Eq. (6b) become

$$\kappa^2\frac{\partial U^{+}}{\partial X_1}+(\kappa^2-2)\frac{\partial V^{+}}{\partial X_3}=\overline{K}_N(1-\epsilon\,\Delta U)\Delta U, \quad 0\leqslant X_3<D, \tag{11}$$

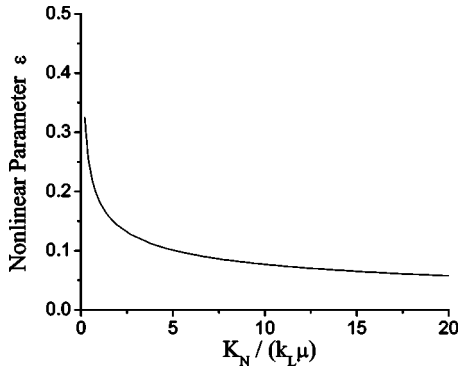

FIG. 2. Nonlinear parameter versus normalized interfacial normal stiffness. The interface is formed by two rough surfaces in contact. The rms roughness of the two surfaces is equal to 0.23 μm, and the material is steel. Further details are to be found in Ref. 13.

$$\frac{\partial U^+}{\partial X_3}+\frac{\partial V^+}{\partial X_1}=\overline{K}_T(1-\epsilon\,\Delta U)\Delta V, \quad 0\leqslant X_3<D, \tag{12}$$

respectively, where $D=k_L d$. In the latter equations, U^+ and V^+ are the normalized total displacement components on the positive side of the crack, while $\overline{K}_N=K_{N,0}/(k_L\mu)$ and $\overline{K}_T=K_{T,0}/(k_L\mu)$ are the normalized normal and tangential interfacial stiffness, where μ is the shear modulus of the material. Finally, $\epsilon=(K_{N,1}/K_{N,0})A_{\rm in}=(K_{T,N}/K_{T,0})A_{\rm in}$ measures the relative variation of the normal and of the tangential interfacial stiffness due to a change of the normal interface opening displacement equal to the amplitude of the incident wave.[13] Note that the proportionality between ϵ and $A_{\rm in}$ implies the quadratic dependence of the amplitude of the actual scattered second harmonic on $A_{\rm in}$. The magnitude of ϵ can be shown to be a monotonically decreasing function of the normalized interfacial stiffness, always being much smaller than one, except for interfaces that are nearly open, for which it tends to diverge. In this work, the dependence of ϵ on the normalized interface stiffness $\overline{K}_N$ is that found by Pecorari[13] for a steel–steel interface between two rough surfaces with rms roughness $\sigma=0.23$ μm (Fig. 2) each, and an incident longitudinal wave with an amplitude $A_{\rm in}=3$ nm. Thanks to this behavior of the nonlinear parameter ϵ, perturbation theory can be used to search for an approximate solution of the problem for nearly all the physically attainable interface conditions. Thus, solutions of the normalized equations of motion are sought in terms of power series of the small parameter ϵ,

$$U(\vec{X},\tau)=U_0(\vec{X},\tau)+\epsilon U_1(\vec{X},\tau)+\cdots, \tag{13}$$

$$V(\vec{X},\tau)=V_0(\vec{X},\tau)+\epsilon V_1(\vec{X},\tau)+\cdots, \tag{14}$$

where the terms proportional to ϵ or its powers play the role of small corrections to U_0 and V_0. By introducing the power series for U and V in the boundary conditions associated to the problem, and regrouping the terms that contain the same power of ϵ, a hierarchy of sets of boundary conditions for U_m and V_m, $m=0,1,...$, is obtained. In particular, the boundary conditions derived from Eqs. (5a)–(5c) for the solutions of the symmetric zeroth-order problem are found to be

$$\frac{\partial U_0^+}{\partial X_3}+\frac{\partial V_0^+}{\partial X_1}=0, \quad X_1=0, \quad 0\leqslant X_3<\infty, \tag{15a}$$

$$\kappa^2\frac{\partial U_0^+}{\partial X_1}+(\kappa^2-2)\frac{\partial V_0^+}{\partial X_3}=\overline{K}_N\,\Delta U_0, \quad 0\leqslant X_3<D, \tag{15b}$$

$$U_0=0, \quad D\leqslant X_3<\infty, \tag{15c}$$

while those for the antisymmetric one are

$$\kappa^2\frac{\partial U_0^+}{\partial X_1}+(\kappa^2-2)\frac{\partial V_0^+}{\partial X_3}=0, \quad X_1=0, \quad 0\leqslant X_3<\infty, \tag{16a}$$

$$\frac{\partial U_0^+}{\partial X_3}+\frac{\partial V_0^+}{\partial X_1}=\overline{K}_T\,\Delta V_0, \quad 0\leqslant X_3<D, \tag{16b}$$

$$V_0=0, \quad D\leqslant X_3<\infty. \tag{16c}$$

Similarly, those for the symmetric first-order problem are

$$\frac{\partial U_1^+}{\partial X_3}+\frac{\partial V_1^+}{\partial X_1}=0, \quad X_1=0, \quad 0\leqslant X_3<\infty, \tag{17a}$$

$$\kappa^2\frac{\partial U_1^+}{\partial X_1}+(\kappa^2-2)\frac{\partial V_1^+}{\partial X_3}=\overline{K}_N\,\Delta U_1-\overline{K}_N\,\Delta U_0^2, \quad 0\leqslant X_3<D, \tag{17b}$$

$$U_1=0, \quad D\leqslant X_3<\infty, \tag{17c}$$

while the boundary conditions for the antisymmetric problem are

$$\kappa^2\frac{\partial U_1^+}{\partial X_1}+(\kappa^2-2)\frac{\partial V_1^+}{\partial X_3}=0, \quad X_1=0, \quad 0\leqslant X_3<\infty, \tag{18a}$$

$$\frac{\partial U_1^+}{\partial X_3}+\frac{\partial V_1^+}{\partial X_1}=\overline{K}_T\,\Delta V_1-\overline{K}_T\,\Delta V_0\,\Delta U_0, \quad 0\leqslant X_3<D, \tag{18b}$$

$$V_1=0, \quad D\leqslant X_3<\infty. \tag{18c}$$

Note the terms $\overline{K}_N\,\Delta U_0^2$ in Eq. (17b) and $\overline{K}_T\,\Delta V_0\,\Delta U_0$ in Eq. (18b) play the role the incident field has in the zeroth-order problem. Being products of solutions of the latter problem, in addition to a time-independent term that is of no importance in the present investigation, these terms contain contributions having a frequency that is twice that of the incident wave. Indeed, the solutions of the equations of motion, Eq. (9) and Eq. (10), having the same period of normalized incident wave, $T=2\pi$, can be expressed as a Fourier series over all the higher harmonics of the fundamental,

$$U(\vec{X},\tau)=\sum_{m=-\infty}^{+\infty}U(\vec{X}|m)\exp(-jm\tau), \tag{19}$$

$$V(\vec{X},\tau)=\sum_{m=-\infty}^{+\infty}V(\vec{X}|m)\exp(-jm\tau), \tag{20}$$

where $m\neq 0$, $\vec{X}=(X_1,X_3)$, and $U(\vec{X}|m)$ and $V(\vec{X}|m)$ are the solutions of the coupled linear differential equations,

$$\frac{\partial^2 U}{\partial X_1^2}+\frac{1}{\kappa^2}\frac{\partial^2 U}{\partial X_3^2}+\left(1-\frac{1}{\kappa^2}\right)\frac{\partial^2 V}{\partial X_1\,\partial X_3}=-m^2U, \tag{21}$$

$$\frac{\partial^2 V}{\partial X_1^2}+\frac{1}{\kappa^2}\frac{\partial^2 V}{\partial X_3^2}+\left(1-\frac{1}{\kappa^2}\right)\frac{\partial^2 U}{\partial X_1\,\partial X_3}=-m^2V. \tag{22}$$

Therefore, the solutions of the mth-order boundary conditions contain harmonic components of order $(m+1)$ at most. The solutions of Eq. (21) and Eq. (22) for the symmetric problem can be expressed as follows:

$$\begin{aligned}U^s(\vec{X}|m)=&\frac{2}{\pi}\int_0^\infty(\zeta A_m^s e^{-m\alpha_L X_3}\\&-2\kappa^{-2}\alpha_T C_m^s e^{-m\alpha_T X_3})\sin(m\zeta X_1)\,d\zeta\\&+\frac{2}{\pi}\int_0^\infty(\alpha_L B_m^s e^{-m\alpha_L X_1}\\&+2\kappa^{-2}\zeta D_m^s e^{-m\alpha_T X_1})\cos(m\zeta X_3)\,d\zeta,\end{aligned} \tag{23}$$

$$\begin{aligned}V^s(\vec{X}|m)=&\frac{2}{\pi}\int_0^\infty(\alpha_L A_m^s e^{-m\alpha_L X_3}\\&-2\kappa^{-2}\zeta C_m^s e^{-m\alpha_T X_3})\cos(m\zeta X_1)\,d\zeta\\&+\frac{2}{\pi}\int_0^\infty(\zeta B_m^s e^{-m\alpha_L X_1}\\&+2\kappa^{-2}\alpha_T D_m^s e^{-m\alpha_T X_1})\sin(m\zeta X_3)\,d\zeta,\end{aligned} \tag{24}$$

while those of the antisymmetric problem are

$$\begin{aligned}U^a(\vec{X}|m)=&\frac{2}{\pi}\int_0^\infty(\zeta A_m^a e^{-m\alpha_L X_3}\\&-2\kappa^{-2}\alpha_T C_m^a e^{-m\alpha_T X_3})\cos(m\zeta X_1)\,d\zeta\\&+\frac{2}{\pi}\int_0^\infty(\alpha_L B_m^a e^{-m\alpha_L X_1}\\&+2\kappa^{-2}\zeta D_m^a e^{-m\alpha_T X_1})\sin(m\zeta X_3)\,d\zeta,\end{aligned} \tag{25}$$

$$\begin{aligned}V^a(\vec{X}|m)=&\frac{2}{\pi}\int_0^\infty(-\alpha_L A_m^a e^{-m\alpha_L X_3}\\&+2\kappa^{-2}\zeta C_m^a e^{-m\alpha_T X_3})\sin(m\zeta X_1)\,d\zeta\\&-\frac{2}{\pi}\int_0^\infty(\zeta B_m^a e^{-m\alpha_L X_1}\\&+2\kappa^{-2}\alpha_T D_m^a e^{-m\alpha_T X_1})\cos(m\zeta X_3)\,d\zeta.\end{aligned} \tag{26}$$

In Eq. (23) to Eq. (26), $A_m^{s,a}$, $B_m^{s,a}$, $C_m^{s,a}$, $D_m^{s,a}$ are unknown functions of ζ to be determined by enforcing the appropriate boundary conditions, and α_L and α_T are defined on the real axis so that

$$\alpha_L=\begin{cases}\sqrt{\zeta^2-1}, & \text{if } \zeta\geqslant 1,\\ -j\sqrt{1-\zeta^2}, & \text{if } \zeta<1,\end{cases}$$

and

$$\alpha_T=\begin{cases}\sqrt{\zeta^2-\kappa^2}, & \text{if } \zeta\geqslant \kappa^2,\\ -j\sqrt{\kappa^2-\zeta^2}, & \text{if } \zeta<\kappa^2.\end{cases}$$

The total components of the normalized displacement fields are recovered from the solution of the symmetric and antisymmetric problems according to the following rules:

$$U(X_1,X_3)=U^s(X_1,X_3)+U^a(X_1,X_3),\quad \text{for } X_1>0,$$

$$U(|X_1|,X_3)=-U^s(|X_1|,X_3)+U^a(|X_1|,X_3),\quad \text{for } X_1<0,$$

$$V(X_1,X_3)=V^s(X_1,X_3)+V^a(X_1,X_3),\quad \text{for } X_1>0,$$

$$V(|X_1|,X_3)=V^s(|X_1|,X_3)-V^a(|X_1|,X_3),\quad \text{for } X_1<0.$$

The details of the mathematical procedure to solve these problems were reported in the work of Achenbach *et al.*[16] and Mendelsohn *et al.*,[17] and will not be repeated here. The only relevant addition to that treatment is the explicit and repeated use of the harmonic balance method to match the time dependence of the scattered field with that of the driving terms given either by the incident field in the boundary conditions for the zeroth-order problems, or by the products of the zeroth-order components in Eq. (17b) and Eq. (18b). The solutions of the zeroth-order problem, thus, can be shown to contain only contributions with the same frequency as the incident field, while those of the first-order system, disregarding a constant term of no interest for the present investigation, describe scattered fields with frequency twice that of the incident wave.

III. NUMERICAL RESULTS

The number of parameters that determine the dynamics of an interface between two rough surfaces in contact is considerable, and that of those that are required to describe the nonlinear scattering of an acoustic wave from a surface-breaking crack with faces in partial contact even more so. As an exhaustive parametric study would go beyond the scope of the present work, the focus here is only on those parameters that most notably affect the detection and localization of the nonlinear defect of interest here. Both shear vertical (SV) and Rayleigh wave incidence are considered next. The frequency of the incident wave is set to be $f=5$ MHz, and the material hosting the crack is steel throughout this work.

A. Shear vertical incidence

SV waves are commonly used for the nondestructive inspection of components in nuclear power plants and in the railway industry when searching for cracks breaking the surface opposite that on which the transmitter in placed. Such waves are often sent into the component along a direction of propagation that forms an angle of 45° with the normal to the surface.

Given the importance of SV waves as a probing tool for surface-breaking cracks, this investigation starts by considering the effect of the angle of incidence, θ_{in}, of such a mode on the acoustic response of a partially closed, surface-breaking crack. The angle of incidence is measured from the x_3 axis, that is to say, from the plane containing the crack. The incident wave is assumed to propagate from infinity toward the stress-free surface with a propagation vector $\vec{k}_T$. In

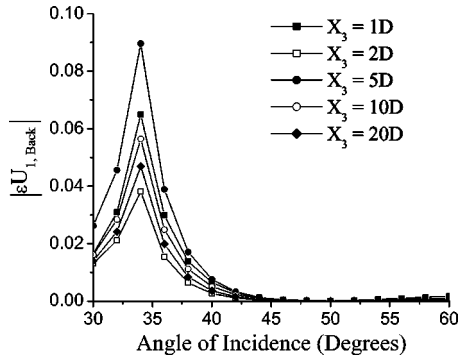

FIG. 3. Normalized backscattered horizontal displacement of the nonlinear field versus the angle of incidence for increasing values of the normalized depth of the observation point. The latter is measured in terms of the normalized crack's depth, D. The normalized crack's depth is $D=0.5$, while $\bar{K}_N=1.95$ and $\epsilon=0.144$.

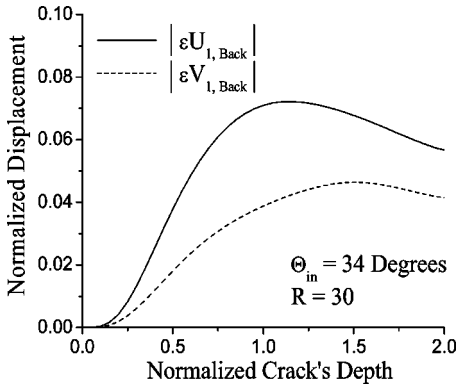

FIG. 4. Normalized backscattered components of the nonlinear displacement as a function of the normalized crack's depth. The angle on incidence is equal to 34°, and the observation point is at a normalized distance, R, equal to 30 from the crack's mouth along the propagation direction of the incident wave. Also, $\bar{K}_N=1.95$ and $\epsilon=0.144$.

all the following simulations, the dependence of the nonlinear parameter ϵ on the interface stiffness is that shown in Fig. 2, and the amplitude of the incident wave, A_{in}, is equal to 3 nm.

Figure 3 shows the dependence on the angle of incidence, θ_{in}, of the horizontal components of the nonlinear backscattered total field at increasing depth within the bulk of the material. A similar behavior is displayed by the vertical components. The angle of incidence is varied by moving the observation point along a surface parallel to the stress-free surface of the half-space. This is done to simulate the common experimental conditions in which the inspecting transducer is moved along a surface that is parallel to that containing the crack. Note that in this and all the subsequent figures the following notation convention has been used: $U(\vec{X}|m)=U_m(\vec{X})$, and $V(\vec{X}|m)=V_m(\vec{X})$. The most relevant feature of Fig. 3 is the marked peak around the critical angle of the longitudinal wave, θ_L, which is equal to 34° in steel. Needless to say, the validity of the considerations that follow does not depend on the specific value of the critical angle, θ_L, which may vary with the material. The enhanced response at θ_L can be easily explained by considering that, at θ_L and in a small neighborhood of it, the amplitude of the reflected longitudinal wave can be considerably larger (in fact, in steel it is 4.3 times larger) than the amplitude of the incident wave. Furthermore, in the neighborhood of θ_L the dominant component of the total incident field is σ_{11}, which, more efficiently than any other, excites the normal vibration mode of the crack. Of relevance because contrary to the assumptions underlying the method most commonly employed to search for surface-breaking cracks is also the considerably smaller response around 45° angle of incidence. Not surprisingly, similar considerations and results are found to hold also for the scattered waves with frequency equal to that of the incident field. Finally, as similarly displayed also in Fig. 5 later, the amplitude of the scattered signal is shown to vary in a nonmonotonic way as the coordinate of the observation point varies.

The effect of the crack's depth on the modulus of the normalized horizontal and vertical displacement components of the second harmonic component is illustrated in Fig. 4. The angle of incidence of the incident SV wave is equal to 34°, while the normalized interface stiffness and the nonlinear parameter are $\bar{K}_N=1.95$ and $\epsilon=0.144$, respectively. The observation point is placed along the direction of propagation of the incident wave at a normalized distance $R=k_L r=30$ from the crack's mouth, where r indicates the actual distance. Results concerning the magnitude of the linear components show the latter to increase up to a value of D of the order of 1.5, after which they remain at the same level for values of D up to 2. This value of D corresponds to an actual crack depth of about $2\lambda_T/3$, where λ_T is the wavelength of the incident wave. The nonlinear components (see Fig. 4), on the other hand, reach their maximum values around $D=1$, after which they tend to decrease, and, similarly to the components of the first harmonics,[17] further oscillate with amplitudes that decrease with increasing crack depth. Deeper cracks are expected to produce nonlinear components having a modulus within the ranges shown in Fig. 4.

The magnitude of the nonlinear response predicted by the model and presented in these examples is large enough that some doubt may be cast on the accuracy of a first-order approximation. A closer examination of the results, however, shows that for smaller values of ϵ corresponding to closer cracks, and at angles of incidence not too close to the critical angle of the longitudinal waves, the magnitude of the second harmonic field generated upon scattering is well within the range of values where the perturbation approach provides accurate results. Indeed, the case of a SV wave incident at 34° is, to some extent, special. To examine this point, the dependence of the ratio between the absolute values of the horizontal displacement of the scattered second and first harmonic components on the normalized crack dimension, D, has been examined for two values of θ_{in}, 45° and 60°, which are commonly used in ultrasonic inspections, as well as for 34°. The results indicate that the response at 45° is always more than 10 dB below that at 34° incidence for all values of the normalized crack, D, less than 2. Similarly, the response at 60° remains considerably below that at 34° incidence for values of $D<1$, and asymptotically approaches the latter for $D>1$. The conclusion to draw from this is that, not only the absolute levels of the linear and nonlinear backscattered fields are higher at the critical angle for longitudinal waves

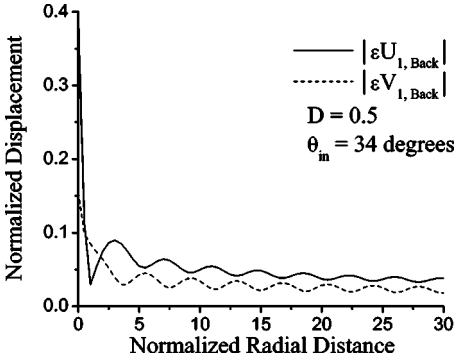

FIG. 5. Normalized backscattered components of the nonlinear field versus distance from the crack's mouth. The observation point is placed along the propagation direction of the incident wave, i.e., $\theta_{\text{in}}=34°$. The normalized crack's depth is $D=0.5$, $K_N=1.95$, and $\epsilon=0.144$.

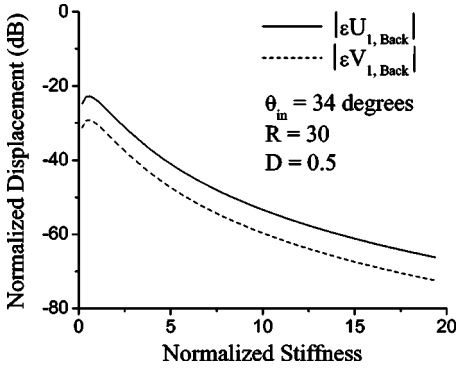

FIG. 6. Normalized backscattered horizontal component of the nonlinear displacement field versus the normalized interfacial stiffness. The normalized distance of the observation point is $R=30$. The remaining system parameters are those of the preceding figure.

than at any other angle of incidence, but also the efficiency of the second harmonic generation is the highest for angles of incidence just above θ_L, especially for cracks with depth $D<1$. In addition, if accurate numerical evaluations of the scattered wave field under these conditions are sought, terms containing higher powers of ϵ should be retained in the perturbation series of Eqs. (13) and (14).

Next, the variation of the modulus of the Cartesian components of the backscattered displacement field with the distance from the crack is considered for a shear wave incident at 34°. The observation point moves along the direction of propagation of the incident wave. The normalized depth of the crack is $D=0.5$, which is approximately equal to $0.15\lambda_T$, while the normalized interface stiffness $K_N=1.95$ and the nonlinear parameter $\epsilon=0.144$. Figure 5 illustrates the dependence of the scattered second harmonic on the distance of the observation point from the crack's mouth, R. The latter moves along the direction of propagation of the incident wave, which is defined by the angle of incidence $\theta_L=34°$. The horizontal component shows a rapid decay to occur within a normalized distance equal to 2 from the crack's mouth, while the vertical component tends to decay more slowly. This behavior may be understood in terms of the increasing constraining effect of the surrounding material on the motion of the particles as the observation point moves away from the surfaces of both the crack and half-space.

Figure 6 shows the variation of the modulus of ϵU_1 and ϵV_1 with the interface closure, i.e., for increasing values of the normalized interface stiffness K_N. The observation point is placed along the backscattering direction at a normalized distance $R=30$ from the crack's mouth. The normalized crack depth is $D=0.5$. After an initial dramatic increase from $-\infty$ corresponding to the formation of first contacts, the modulus of the Cartesian nonlinear components decay in a monotonic fashion that strongly resembles that predicted for the nonlinear response on an infinite interface.

In the introduction, results obtained by Krohn *et al.*[6] were reported for their relevance to the issue of defect location by means of nonlinear ultrasonic techniques. In particular, it was mentioned that using laser interferometric detection, a highly localized nonlinear response of delaminations could be detected within thin composite plates. It was also reported that, so far, no convincing explanation for such a strong localization has been found, although some form of trapping mechanism of the energy carried by the higher harmonic wave has been hypothesized.[18] Although apparently simplistic, two remarks are in order. The first concerns the detection technique employed in that work, which is sensitive to the displacement component normal to the inspected surface. The second remark regards the fact that the delamination is likely to be roughly parallel to the surface on which the measurements are carried out. Therefore, considering that in the experiments mentioned above the wavelength of the acoustic excitation is much larger than the plate's thickness, it is reasonable to conceive that the behavior of the normal component of the displacement of the higher harmonic wave detected at the stress-free surface closely resembles the normal crack opening displacement. Calculations have been carried out with this model and presented in Fig. 7, which illustrates the dependence of ϵU_1, that is to say, the nonlinear displacement component normal to the crack surface, on the coordinate X_3 at $X_1=0^-$. The crack's normalized depth is $D=0.5$, the normalized interface stiffness and nonlinear parameter are $K_N=1.95$ and $\epsilon=0.144$, respectively. A sudden drop of the modulus of ϵU_1 is observed at the crack tip, which exceeds 30 dB. This prediction of the model suggests that the highly localized nonlinear response detected by the interferometric technique follows the spatial dependence of

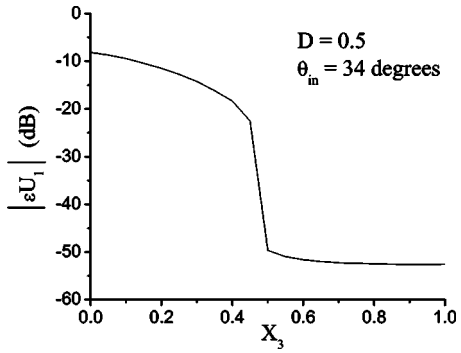

FIG. 7. The dependence of the normalized nonlinear component of the displacement normal to the crack on X_3 for $X_1=0$. The system parameters are those of Fig. 5.

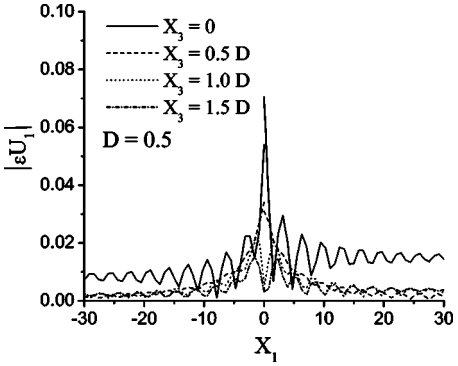

FIG. 8. Normalized backscattered horizontal displacement of the nonlinear field versus X_1 at four different values of X_3. The latter is measured in terms of normalized crack's depth, D. The normalized crack's depth is $D=0.5$, while $\overline{K}_N=1.95$ and $\epsilon=0.144$.

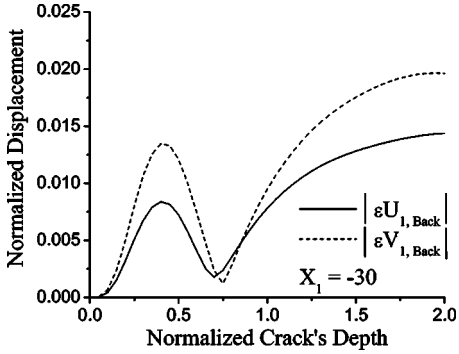

FIG. 9. Normalized backscattered components of the nonlinear field versus the normalized crack's depth. The observation point is placed on the surface of the half-space at a normalized distance $X_1=-30$. The normalized crack's depth is $D=0.5$, $\overline{K}_N=1.95$, and $\epsilon=0.144$.

the normal component of the opening displacement of the delamination.

Finally, it should be remarked that, for all the cases considered so far, very similar theoretical results have been obtained for the same field variables in the forward scattering direction, and, for this reason, they have not been presented here.

B. Rayleigh wave incidence

The case of a Rayleigh wave insonifying a partially closed surface-breaking crack is considered next. The amplitude of the horizontal displacement component of the incident wave at the stress-free surface is chosen to be equal to 3 nm: $u_{\text{in}}(x_1,x_3=0)=3$ nm.

Figure 8 illustrates the behavior of the modulus of the second harmonic component of the horizontal displacement at four values of the depth, X_3, as a function of the variable X_1. The dependence of the first harmonic component displays features similar to those of the second harmonic, and, therefore, is not shown here. The normalized crack's depth is $D=0.5$, and the interfacial stiffness and the nonlinear parameter are again $\overline{K}_N=1.95$ and $\epsilon=0.144$. As in the case of SV incidence, in the plane $X_1=0$ the displacement component normal to the crack's plane undergoes a dramatic and sudden drop at the tip of the crack. The forward scattered second harmonic wave is also shown to approach an average value slightly higher than that of the backward scattered component as the value of X_1 increases in both directions.

The effect of the interface closure on the modulus of both vertical and horizontal second harmonic components of the displacement field is also investigated. The behavior of these components is found to closely resemble that already seen in Fig. 6.

Finally, Fig. 9 and Fig. 10 show the backward and forward normalized Cartesian components of the nonlinear scattered field, respectively, at a distance $|X_1|=30$ on the surface of the half-space as functions of the normalized crack's depth, D. The values of the interfacial stiffness and of the nonlinear parameter are those already used in Fig. 8. A remarkable difference of behavior between the forward and the backward components can be easily noticed, as the former increases nearly monotonically with the crack's depth up to $D\approx 1$ to remain roughly at the same level afterward, while the latter displays pronounced interference features for values of $D<1$. Worth noting is also the considerably higher values of the forward scattered field compared to that scattered in the opposite direction.

IV. SUMMARY AND CONCLUDING REMARKS

A theoretical model that predicts the generation of the second harmonic component upon scattering of an incident harmonic wave by a surface-breaking crack with faces in partial contact has been presented. The cases of shear vertical and Rayleigh wave incidence have been considered, and for each, the effect of parameters such as the angle of incidence, the crack's depth, and the crack's closure on the nonlinear response of the crack have been examined. The nonlinearity of the scattering defect has been introduced into the mathematical formulation of the problem by extending the boundary conditions at the crack's contacting faces to account for the nonlinear effect of the two-dimensional distribution of elastic contacts. It has been shown that when cracks with depth not larger than λ_T are insonified by a shear vertical wave, the highest linear and nonlinear responses of such defects occur when the latter are insonified at an angle slightly higher than the critical angle of the longitudinal wave, θ_L. Further, the generation of the second harmonic has been found to be the most efficient in such a configuration. The

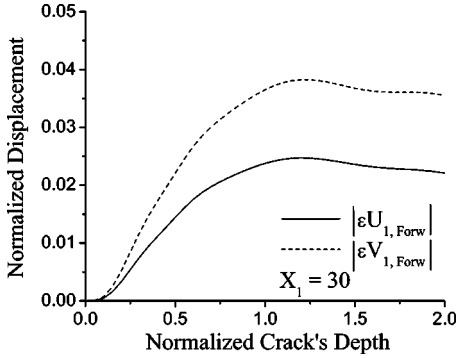

FIG. 10. Normalized forward scattered components of the nonlinear field versus the normalized crack's depth. The observation point is placed on the surface of the half-space at a normalized distance $X_1=30$. The normalized crack's depth is $D=0.5$, $\overline{K}_N=1.95$, and $\epsilon=0.144$.

relevance of this finding stems in part from the fact that they force us to reconsider the suitability of the inspection methods currently used to search for surface-breaking cracks utilizing SV waves at 45° incidence, regardless of the depth of the crack sought and the hosting material. As demonstrated in this work, the sensitivity of a SV wave inspecting such defects at 45° incidence is much lower than that at and just above θ_L. This problem is further investigated elsewhere.[19]

An additional important advantage offered by the use of SV waves at or just above θ_L concerns the localization of a defect. In fact, the exploitation of the efficient mode conversion of the incident SV wave into an evanescent longitudinal wave propagating along the surface renders this configuration considerably more sensitive to crack-like defects located at the surface of the sample than to any other defect placed along the direction of propagation of the incident field. Therefore, in search of surface-breaking cracks that are located on the surface opposite that which is scanned by an ultrasonic probe by means of both linear and nonlinear scattering techniques employing beams of finite lateral dimensions, the setup providing the highest sensitivity offers also a solution to the localization problem.

Of further concern to the localization problem, the model presented here suggests a simple and plausible interpretation of recent experimental results by Krohn *et al.*[6] showing a highly localized nonlinear response of delaminations in composite materials. In fact, the model indicates that the experimental observations capture the very rapid decay of the nonlinear opening displacement normal to the delamination occurring beyond the borders of the latter. The model predicts a magnitude of such a drop to be of the order of 30 dB, which exceeds the experimentally observed behavior by at least 10 dB. A possible reason for such an overestimation may be the asymmetric position of the actual delamination within the plate's cross section. In fact, if located outside the midplane of the plate, the crack is expected to generate a scattered field that cannot be decomposed into symmetric and antisymmetric parts, the former yielding a nearly null contribution to the component of the displacement field normal to the plane containing the crack [Eq. (17c)].

Finally, for both SV and Rayleigh wave incidence, the magnitude of the nonlinear response displays a similar behavior with respect to variations of the interfacial stiffness. After reaching an absolute maximum for values of the normalized stiffness proximal to 1, they monotonically decay for increasing values of K_N, as has already been noticed in the case of an infinite interface formed by rough surfaces in contact.

ACKNOWLEDGMENTS

This work was supported by the Swedish Inspectorate for Nuclear Power (SKI), under Contract No. 14.43-010902,01156, and by the Swedish Center for Nuclear Technology under the contract entitled ''Detection of stress-corrosion cracks by means of nonlinear scattering of ultrasonic waves.''

[1] I. Y. Solodov, ''Ultrasonics of non-linear contacts: propagation, reflection and NDE applications,'' Ultrasonics **36**, 383–390 (1998).
[2] I. Y. Solodov, N. Krohn, and G. Busse, ''CAN: an example of non-classical acoustic nonlinearity in solids,'' Ultrasonics **40**, 621–625 (2002).
[3] I. Y. Solodov and B. A. Korshak, ''Instability, chaos, and 'memory' in acoustic wave–crack interaction,'' Phys. Rev. Lett. **88**, 014303 (2002).
[4] V. Y. Zaistev, V. Gusev, and B. Castagnede, ''Observation of the 'Luxenburg–Gorky' effect for elastic waves,'' Ultrasonics **40**, 627–631 (2002).
[5] V. Y. Zaistev, V. Gusev, and B. Castagnede, ''Luxenburg–Gorky effect retooled for elastic waves: a mechanism and experimental evidence,'' Phys. Rev. Lett. **89**, 105502 (2002).
[6] N. Krohn, R. Stoessel, and G. Busse, ''Acoustic non-linearity for defect selective imaging,'' Ultrasonics **40**, 633–637 (2002).
[7] J. D. Achenbach and A. N. Norris, ''Loss of specular reflection due to nonlinear crack–face interaction,'' J. Nondestruct. Eval. **3**, 229–239 (1982).
[8] S. Hirose and J. D. Achenbach, ''Higher harmonics in the far field due to the dynamic crack–face contacting,'' J. Acoust. Soc. Am. **93**, 142–147 (1993).
[9] S. Hirose, ''2-D scattering by a crack with contact boundary conditions,'' Wave Motion **19**, 37–49 (1994).
[10] D. Donskoy, A. Sutin, and A. Ekimov, ''Nonlinear acoustic interaction on contact interfaces and its use for nondestructive testing,'' NDT & E Int. **34**, 231–238 (2001).
[11] J. M. Baik and R. B. Thompson, ''Ultrasonic scattering from imperfect interfaces: a quasi-static model,'' J. Nondestruct. Eval. **4**, 177–196 (1984).
[12] C. Pecorari, ''Scattering of a Rayleigh wave by a surface-breaking crack with faces in partial contact,'' Wave Motion **33**, 259–270 (2001).
[13] C. Pecorari, ''Nonlinear interaction of plane ultrasonic waves with an interface between rough surfaces in contact,'' J. Acoust. Soc. Am. **113**, 3065–3072 (2003).
[14] K. L. Johnson, *Contact Mechanics* (Cambridge University Press, New York, 1985).
[15] R. D. Mindlin and H. Deresiewicz, ''Elastic spheres in contact under varying oblique forces,'' J. Appl. Mech. **20**, 327–344 (1953).
[16] J. D. Achenbach, L. M. Keer, and D. A. Mendelsohn, ''Elastodynamic analysis of an edge crack,'' J. Appl. Mech. **47**, 551–556 (1980).
[17] D. A. Mendelsohn, J. D. Achenbach, and L. M. Keer, ''Scattering of elastic waves by a surface-breaking crack,'' Wave Motion **2**, 277–292 (1980).
[18] I. Y. Solodov, ''Ultrasonics of nonlinear interfaces in solids: new physical aspects and NDE applications,'' *Proceedings of the 5th Ultrasonics World Conference*, 2003, pp. 555–564.
[19] C. Pecorari, ''A note on the sensitivity of SV wave scattering to surface-breaking crack,'' to appear in Ultrasonics.

PAPER C

SO, . . . IS THIS A SURFACE-BREAKING CRACK?

Milan Poznic, Claudio Pecorari*
Marcus Wallenberg Laboratory
Royal Institute of Technology
100 44 Stockholm, Sweden

An inspection technique used to assess the structural integrity of critical components in a nuclear power plant must be able to discern cracks that are surface-breaking from those which are subsurface. This work presents a theoretical investigation on an ultrasonic method which is conceived to provide that information. The main assumption of the model is that water carried by pressurized pipes infiltrates and fills a surface-breaking crack, while a subsurface crack is dry. The model simulates an inspection in which the modulation technique is employed and the surface hosting the crack is not accessible. A ratio, *R*, constructed with signals recorded in backscattering configuration during a modulation cycle, is examined and shown to provide a clear criterion to distinguish subsurface from surface-breaking cracks when a shear vertical wave at 45 degree incidence is employed as a probe.

(*) Corresponding author (pecorari@kth.se)

(submitted to the Journal of Mechanics of Materials and Structures)

1. Introduction

Stress corrosion cracks, especially in pipes carrying pressurized water, constitute a serious threat to the structural integrity of nuclear power plants. They are often found in regions proximal to the inner surface of the pipe, and can be either surface-breaking or subsurface. In the latter case, of the two mechanisms leading to crack growth, fatigue is the one which dominates. When breaking the surface of the hosting component, the balance between these mechanisms changes dramatically. In fact, the combination of tensile stresses, which maintain a crack open while the plant is operating, and the pipe

internal pressure, which can reach values of the order of 70 Atm, often result in water entering the fracture and accelerate the corrosion cracking.

For this reason, it is of the outmost importance for a nondestructive technique employed in the assessment of a plant's structural integrity to enable not only the detection of stress-corrosion cracks, but also their characterization as surface-breaking or subsurface defects. Indeed, there have been instances in which cracks with small but still finite size ligaments separating them from the inner surface of the pipe were characterized as subsurface during inspection but were proved to be surface-breaking upon a destructive metallurgical investigation [Jenssen *et al*. 2000]. Of relevance to the subject of this work is also the presence of debris resulting from corrosion, which tends to bridge the gap between the surfaces rendering the defect more transparent to an inspecting ultrasonic beam.

This work presents the principles of an ultrasound-based technique designed to discern partially closed cracks which are subsurface from those that are surface-breaking. The proposed method exploits the effects of water confined within a partially closed, surface-breaking crack on the acoustic response of the defect. The sensitivity of the proposed technique to the presence of fluid trapped between the crack faces, and to compressive stresses acting on the crack is examined. The emphasis on cracks that are partially closed derives from the nearly certain event that, following the shut-down of the plant prior to inspection, stresses due to the plant's operating conditions are removed and cracks tend to partially close, at least in proximity of their tips (see for example Newman *et al*. 2003). The investigation is limited to the worst case scenario in which the surface hosting the crack is not accessible and the inspection must be carried out from the outer surface of the component.

The content of this communication is organized as follows. First, experimental results which illustrate the characteristic dependence of the stiffness on the pressure applied to dry and fluid filled interfaces are reported. Secondly, a model which evaluates the backscattering by partially closed, surface-breaking and subsurface cracks is presented. To simulate the effect of partial closure on backscattering, the spring boundary conditions are employed. The results obtained on partially closed interfaces are utilized in the theoretical model to describe the effect of water trapped within a surface-breaking

fracture. Next, numerical results obtained by simulating an experiment in which the partial closure of the crack is modulated by a low frequency, high amplitude wave while a probing ultrasonic wave interrogates the defect are reported. A discussion of the significance of these findings to the development of a method which allows water-confining surface-breaking cracks and dry subsurface cracks to be distinguished from each other ends this communication.

2. Dry and water-confining interfaces

The interaction between ultrasonic waves and interfaces formed by two rough, nonconforming surfaces in contact under increasing pressure has been investigated extensively both experimentally and theoretically by several authors (among the many Baltazar *et al.* 2002, Baik and Thompson 1984, Drinkwater et al. 1996, Kim, A. Baltazar, and S.I. Rokhlin 2004, Nagy 1992). Models have been developed which derive the macroscopic mechanical properties of such interfaces from those of the asperities in contact and from the topographical properties of the surfaces. This considerable effort notwithstanding, several are the outstanding issues concerning this problem still waiting for a solution (Pecorari and Poznic (*to be published)*). In particular, the effect of water confined between surfaces in partial contact appears not to be accounted for by any of the models currently available.

In this section, experimental results on both dry and water-confining interfaces are presented and later used in the theoretical model describing ultrasonic wave scattering by surface-breaking and subsurface cracks. The experimental set-up employed in this investigation has been discussed elsewhere (Pecorari and Poznic (*to be published)*) and for this reason it is not repeated here. The only noteworthy differences with earlier work concern *i.* the nominal frequency of the transducer used to generate and receive the waves reflected by the imperfect interface, which is equal to 2.25 MHz in the present investigation, *ii*. measurements have been carried out also with shear waves, and *iii*. the rms roughness of the two surfaces employed here was evaluated to be of the order of 0.2 μm. In all the measurements, the inspecting waves insonify the interface at normal incidence.

Among the properties of interest, the stiffness of the imperfect interface, *K*, defined by the relationship, $K = \partial P / \partial \delta$, where P is the applied pressure and δ is the relative approach between the mean planes of the rough surfaces, is of primary importance to understand the interaction between ultrasonic waves and such interfaces. The values of the normal and transverse interfacial stiffness, $K_{N,T}$, can be recovered from the measured reflection coefficients for longitudinal and shear waves at normal incidence, $R_{L,T}$, by using the well-known relationship

$$R_{L,T} = -\frac{1}{1 - 2j\left(K_{N,T} / \omega Z_{L,T}\right)}. \tag{2-1}$$

In eq. (2-1), ω is the circular frequency of the incident and scattered waves, and $Z_{L,T}$ are the acoustic longitudinal and shear impedances of the medium, respectively. The symbol *j* represents the imaginary unit. When water is confined by the interface, the normal stiffness of the latter can be written as the sum of two terms: $K_N = \left(\Lambda / d_0\right) + \Delta K_N$. The first term describes the effect of a layer of water with thickness d_0, the latter quantity being the distance between the mean planes of the rough surfaces when no pressure is applied to the interface. The symbol Λ represents the only nonzero elastic constant of the liquid medium. The second term, ΔK_N, describes the part of the stiffness which depends on the applied pressure. Since the shear modulus of water is zero, the transverse stiffness does not contain a term analogous to Λ / d_0.

Figure (1a, b) illustrates the dependence of the normalized normal, $K_N / \omega Z_L$, and transverse, $K_T / \omega Z_L$, interface stiffness on the applied pressure for both dry and water-confining interface, respectively. The pressure is varied from 0 MPa to 80 MPa at which point the reflection coefficient of a longitudinal wave interacting of a water-confining interface is smaller than 0.1. The two most relevant features of Figure 1a are the overall larger normal stiffness of the water-confining interface compared to that of the dry one, and the initial fast increase of K_N when pressure not exceeding 5 MPa is applied to the interface. Both experimental and theoretical investigations on the interaction between solid surfaces confining water would suggest that repulsive forces arising when the liquid

is confined within spaces with dimensions comparable to the diameter of the liquid molecules, may be responsible for the observations reported in Figure (1) [Das *et al.* 1996, Israelashvili 1992, Grabbe and Horn 1993, Ho *et al.* 1998, Pashley and Israelashvili 1984]. Of importance is also the identity of the results concerning the shear stiffness, K_T, which have been obtained with the same two interfaces (see Figure 1b). In summary, these results show that water strongly affects the dependence of the interface normal stiffness on the applied pressure, while it does not alter that of the shear stiffness.

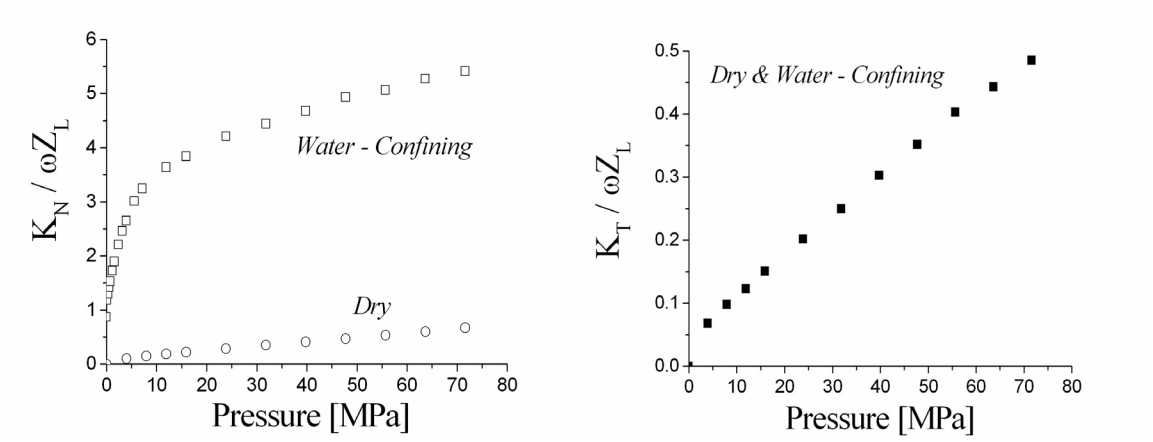

Figure 1. *a) Normalized normal, K_N, and b) transverse, K_T, spring stiffness versus pressure applied to a water-confining and dry steel-steel interface.*

3. Theory

Figure 2 illustrates the geometry of the material system and of the defect under consideration. With reference to it, and following the method developed by Achenbach *et al.* [1980] and Mendelsohn *et al.* [1980], the original problem posed by the scattering of an incident bulk wave onto the crack is decomposed into a symmetrical and an antisymmetrical part.

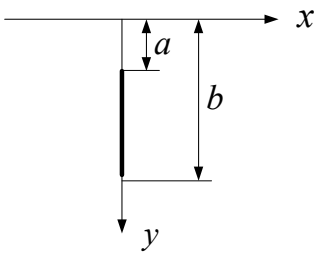

Figure 2. *Geometry of the material system and of its defect. The material system occupies the halfspace y > 0. For a surface-breaking crack a = 0.*

When considering the scattering by a subsurface crack, the boundary conditions associated with the symmetrical problem are

$$\text{(3-1.a)} \qquad \sigma_{xy}^{+} = 0\,, \qquad x = 0,\ 0 \le y < \infty\,,$$

$$\text{(3-1.b)} \qquad \sigma_{xx}^{+} = K_N\,\Delta u\,, \qquad a \le y < b\,,$$

$$\text{(3-1.c)} \qquad u = 0, \qquad 0 \le y < a,\ \ b \le y < \infty\,,$$

and those associated to the antisymmetrical problem are

$$\text{(3-2.a)} \qquad \sigma_{xx}^{+} = 0\,, \qquad x = 0,\ 0 \le y < \infty\,,$$

$$\text{(3-2.b)} \qquad \sigma_{xy}^{+} = K_T \Delta v\,, \qquad a \le y < b\,,$$

$$\text{(3-2.c)} \qquad v = 0, \qquad 0 \le y < a,\ \ b \le y < \infty.$$

In eqs. (3-1) and (3-2), σ_{ii}^{+} are the total stresses acting on the positive side of the crack, i.e., on the side for which $x = 0^{+}$, while u and v are the displacement components in the x and y direction, respectively. The spring stiffness densities K_N and K_T are generally allowed to be functions of depth, y, so that nonuniform closure can be modeled. The crack closure is simulated by varying the contact pressure between the crack faces according to the following equations which are given next only for a subsurface crack

$$\text{(3-3.a)} \qquad P(y) = P_{tip}\,\exp\!\left[(y-b)/\ell\right], \qquad (a+b)/2 \le y \le b\,,$$

$$\text{(3-3.b)} \qquad P(y) = P_{tip}\,\exp\!\left[-(y-a)/\ell\right], \qquad a \le y \le (a+b)/2\,.$$

In eq. (3-3), P_{tip} is the pressure at the crack tips and ℓ is the decay length which controls the spatial extent of the tip closure. The pressure distribution on a surface-breaking crack is obtained from eq. (3-3) by letting $a = 0$. Equations (3-3a,b) are used to assign a local value of the spring stiffness densities by way of the relationships illustrated in Figure 1. The purpose of this feature of the model is twofold. First of all, the effect of the water on the scattering phenomenon is accounted for within the same mathematical scheme used to treat a dry partially closed crack. Secondly, the boundary conditions in eqs. (3-1) and (3-2) allow for the simulation of the well documented of closure of a crack in the regions proximal to its tips [Newman *et al*. 2003], the causes of which are varied, still debated,

and leading essentially to the same result when considered from the wave scattering point of view. The equations of motion for the two components displacement components are

$$c_L^2 \frac{\partial^2 u}{\partial^2 x} + c_T^2 \frac{\partial^2 u}{\partial^2 y} + \left(c_L^2 - c_T^2\right)\frac{\partial^2 v}{\partial x \partial y} = \frac{\partial^2 u}{\partial^2 t}, \tag{3.4.a}$$

$$c_L^2 \frac{\partial^2 v}{\partial^2 x} + c_T^2 \frac{\partial^2 v}{\partial^2 y} + \left(c_L^2 - c_T^2\right)\frac{\partial^2 u}{\partial x \partial y} = \frac{\partial^2 v}{\partial^2 t}, \tag{3-4.b}$$

where t represents time, and c_L and c_T are the phase velocities of longitudinal and shear waves, respectively. The solutions of these are given by the following expressions [Achenbach *et al.* 1980, and Mendelshon *et al.* 1980]

$$\begin{aligned} u^s(\vec{x}) = {} & \frac{2}{\pi}\int_0^\infty \left(\xi k_L A^s e^{-\alpha_L k_L y} - 2\kappa^{-2}\alpha_T k_L C^s e^{-\alpha_T k_L y}\right)\sin\left(\xi k_L x\right) d\xi + \\ & \frac{2}{\pi}\int_0^\infty \left(\alpha_L k_L B^s e^{-\alpha_L k_L x} + 2\kappa^{-2}\xi k_L D^s e^{-\alpha_T k_L x}\right)\cos\left(\xi k_L y\right) d\xi \end{aligned}, \tag{3-5.a}$$

$$\begin{aligned} v^s(\vec{x}) = {} & \frac{2}{\pi}\int_0^\infty \left(\alpha_L k_L A^s e^{-\alpha_L k_L y} - 2\kappa^{-2}\xi k_L C^s e^{-\alpha_T k_L y}\right)\cos\left(\xi k_L x\right) d\xi + \\ & \frac{2}{\pi}\int_0^\infty \left(\xi k_L B^s e^{-\alpha_L k_L x} + 2\kappa^{-2}\alpha_T k_L D^s e^{-\alpha_T k_L x}\right)\sin\left(\xi k_L y\right) d\xi \end{aligned}, \tag{3-5.b}$$

for the symmetric field, while those of the antisymmetric are

$$\begin{aligned} u^a(\vec{x}) = {} & \frac{2}{\pi}\int_0^\infty \left(\xi k_L A^a e^{-\alpha_L k_L y} - 2\kappa^{-2}\alpha_T k_L C^a e^{-\alpha_T k_L y}\right)\cos\left(\xi k_L x\right) d\zeta + \\ & \frac{2}{\pi}\int_0^\infty \left(\alpha_L k_L B^a e^{-\alpha_L k_L x} + 2\kappa^{-2}\xi k_L D^a e^{-\alpha_T k_L x}\right)\sin\left(\xi k_L y\right) d\xi \end{aligned}, \tag{3-6.a}$$

$$\begin{aligned} v^a(\vec{x}) = {} & \frac{2}{\pi}\int_0^\infty \left(-\alpha_L k_L A^a e^{-\alpha_L k_L y} + 2\kappa^{-2}\xi k_L C^a e^{-\alpha_T k_L y}\right)\sin\left(\xi k_L x\right) d\xi - \\ & \frac{2}{\pi}\int_0^\infty \left(\xi k_L B^a e^{-\alpha_L k_L x} + 2\kappa^{-2}\alpha_T k_L D^a e^{-\alpha_T k_L x}\right)\cos\left(\xi k_L y\right) d\xi \end{aligned}. \tag{3-6.b}$$

In the above equations, $A^{a,s}$, $B^{a,s}$, $C^{a,s}$, and $D^{a,s}$ are functions of the integration variable, ξ, and are themselves given in terms of integrals of suitable functions containing the tangential slope of the two components of the crack opening displacement. These are

obtained by solving two decoupled singular integral equations derived by enforcing the boundary conditions (3-1.a-c) and (3-2.a-c) on the solutions of the equations of motion. The symbols k_L and k_T are the wavenumbers of the longitudinal and shear waves, respectively. With the same meaning of the subscripts L and T, the quantities α_L and α_T are defined by

$$(3\text{-}7) \qquad \alpha_L = \begin{cases} \sqrt{\xi^2 - k_L^{\,2}}, & if\ \ \xi \geq k_L \\ -j\sqrt{k_L^{\,2} - \xi^2}, & if\ \ \xi < k_L \end{cases} \quad \text{and} \quad \alpha_T = \begin{cases} \sqrt{\xi^2 - k_T^2}, & if\ \ \xi \geq k_T \\ -j\sqrt{k_T^2 - \xi^2}, & if\ \ \xi < k_T \end{cases}$$

The branch of the square root function in the complex plane is chosen to satisfy the Sommerfeld radiation condition. Equations (3-5) and (3-6) concern the field in the quarterspace for which both x and y are positive. The field components in the quarterspace for which $x < 0$ are obtained from those given by eq. (3-5) and (3-6) according to the following rules

$$(3\text{-}8.a) \qquad u^s(x<0,y) = -u^s(|x|,y),$$

$$(3\text{-}8.b) \qquad v^s(x<0,y) = v^s(|x|,y),$$

$$(3\text{-}8.c) \qquad u^a(x<0,y) = u^a(|x|,y),$$

$$(3\text{-}8.d) \qquad v^a(x<0,y) = -v^a(|x|,y).$$

In solving the integral equations in the unknown tangential slope of two components of the displacement discontinuity, the conditions that their integral over the extent of the crack is null must be enforced. The scattering by an open subsurface crack was solved first by Brind and Achenbach [1981].

The scattering from a partially closed, surface-breaking crack is modeled within the same mathematical framework. The boundary conditions for this problem are obvious extensions of those given for a surface-breaking crack, and the solutions of the problem are again sought in the form given by eqs. (3-5) and (3-6).

4. Numerical results

The experimental results of Section 2 indicate that the most striking difference between the properties of two interfaces under consideration is the rapid increase of the normal stiffness of the water-confining interface as soon as contact between asperities is established. This naturally suggests the use of the parametric modulation technique as a novel method to characterize a crack as being surface-breaking or subsurface. The modulation technique exploits the nonlinear properties of partially closed cracks, and more specifically the dependence of the crack stiffness on the applied pressure. Xiao and Nagy [1998] employed thermal stresses induced by a laser source to vary the closure of a surface-breaking crack which was simultaneously insonified by a high frequency Rayleigh wave. By means of suitable signal processing of the backscattered ultrasonic pulse acquired during different phases of the thermal modulation, Xiao and Nagy showed that the acoustic signature of the crack can be extracted from the noisy environment. In other words, the modulation technique was shown to be able to selectively detect nonlinear material defects. Rokhlin *et al.* [2004] adapted this method to increase the sensitivity of ultrasonic inspections to poor adhesive bonds between aluminum plates, while Kim, Yakovlev, Rokhlin [2004] (and references therein) used it to characterize small surface-breaking crack initiated at surface pits by fatigue. Finally, Kazakov *et al.* [2002] used the same idea to image the nonlinear properties of a surface-breaking crack. Rokhlin *et al.*, Kim *et al.*, and Kazakov *et al.* used a low frequency source of mechanical vibrations to vary the instantaneous properties of the defect of interest.

In this work, an experimental configuration similar to those employed by the previously cited authors is simulated (see Figure 3). A crack under investigation is subjected to a sinusoidal, time-dependent pressure field of amplitude ΔP: $P(t) = \Delta P \sin(\Omega t)$, the frequency of the modulation, Ω, being order of magnitude lower than that of an ultrasonic wave, ω, which is used to monitor the instantaneous state of the crack. During a cycle, three backscattered ultrasonic signals are recorded, two at the opposite turning points of each cycle, and one at the mid point when $P(t) = 0$. By using the peak-to-peak amplitude, or any other feature of the backscattered signal which reflects the variation of the crack state, the following ratio is

constructed: $R = \left(B^- - B^+\right)/B_o$, where $B^{-,+}$ are the features of interest measured when the crack is most open (-) or closed (+), respectively, and B_o refers to the crack state in its rest condition. Note that the ratio R is independent of the amplitude of the incident wave, and, thus, conveys information which depends on the intrinsic properties of the defect but not on the intensity of the inspecting wave. This work investigates the conditions under which R can possibly serve as an "index of state" to distinguish a fluid filled surface-breaking crack from a dry subsurface crack.

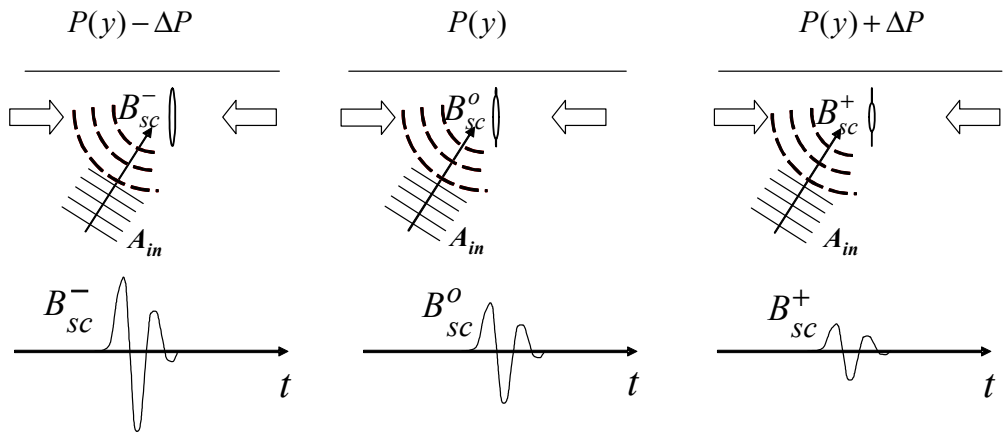

Figure 3. *Schematics of the simulated modulation experiment illustrating the relationship between the state of the crack and the signal backscattered by it during a cycle of the modulation.*

The following numerical investigation considers the scattering by partially closed surface-breaking and subsurface cracks in a steel halfspace. The mass density and phase velocity of longitudinal and shear waves in steel are ρ = 7.8 $\times 10^3$kg m^{-3}, c_L = 5800 ms^{-1}, and c_T = 3200 ms^{-1}. The results presented in all the following figures refer to a configuration in which a shear vertical wave impinges on the defect at 45 degree incidence. The frequency of the wave is f = 2.25 MHz. The solution of the scattering problem is evaluated in the backscattering direction. The observation point lies at a distance of about 30 shear wavelengths (about 40 mm) from the surface of the halfspace. The residual pressure which determines the closure of the crack (see eq. (3-3)) is chosen to represent three characteristic configurations: one in which the closure is uniform, and two in which it decays with rates equal to 0.1 mm and 1 mm, respectively. The rationale behind the choice of the latter values stems from the assumption that the cracks of

interest are detectable by conventional methods, and, thus, their extent is of the order of several millimeters. For such cracks a likely state is one in which their tip(s) are partially closed while throughout the remaining portion of their extent there is no mechanical contact between the surfaces. The pressure at the crack tip, P_{tip}, is chosen to be equal to 5 MPa and 70 MPa to represent two well distinct situations in which the crack tip is nearly open or fairly closed, respectively. The values of the normalized stiffness constants $K_N/(\omega Z_L)$ and $K_T/(\omega Z_L)$ corresponding to these pressure values are 0.2 and 0.07, respectively, if the crack is dry, and 3 and 0.07 if a defect contains water. The amplitude of the modulation is ΔP = 5 MPa in all simulations. The dependence of the ratio R on the nondimensional size of the crack, $k_T d$, is reported over a range which corresponds to cracks with physical dimension reaching values up to 5.36 mm.

Figure (4a) refers to a dry surface-breaking crack and Figure (4b) to the same crack when it is filled with water. In both figures, the cases in which the crack is subjected to a uniform pressure, P_{tip}, of 5 MPa and 70 MPa are considered. In Figure (4a), the crack shows a nearly constant response when P_{tip} = 70 MPa, reflecting the modest effect the modulation has on the crack opening, while it displays wide oscillation for the lower value of the applied pressure. In both cases, however, the ratio R does not exceeds values of 0.1 as the size of the crack increases. If water is confined within the crack (see Figure 4b), the value of the ratio for P_{tip} = 70 MPa is even smaller as a consequence of the higher values of the crack stiffness, while for P_{tip} = 5 MPa R reaches values larger than 2

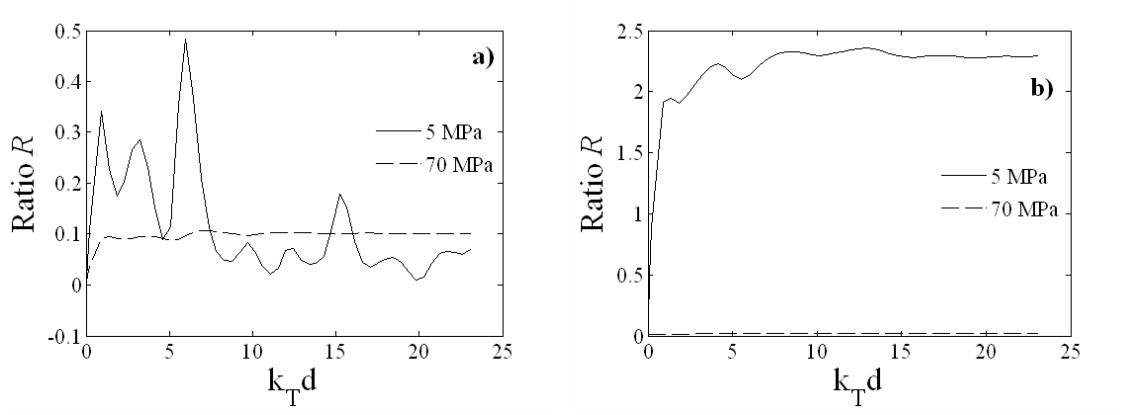

Figure 4. *Ratio, R, versus nondimensional crack size $k_T d$ for values of the pressure at the crack tip equal to 5 MPa and 70 MPa. The pressure distribution is constant along the crack extent: a) dry surface-breaking crack, b) water-confining surface-breaking crack.*

over nearly all the range of values of $k_T d$ considered here. This striking contrast is due to the large variation of values spanned by the normal stiffness as the total applied pressure varies between 0 and 10 MPa (see Figure 1a).

Figure (5a,b) illustrates the dependence of the ratio R for a surface-breaking crack with a closure which is given by eqs. (4), specified for the case of a surface-breaking crack ($a = 0$), and with $\ell = 1$ mm. As in the case considered in Figure (4a), the response of a dry surface-breaking crack tends to settle around values of the order of 0.1 as the size of he crack increases. However, a water-confining crack which is subjected to a compressive stress of 70 MPa at its crack tip (Figure 5b) displays a remarkably different behavior compared to that shown in Figure (4b). In fact, as the crack size exceeds the decay length, ℓ, the ratio rapidly increases to reach values larger one. This prediction can be explained as the result of an increasingly larger portion of the crack surface being subject to an external pressure smaller than the amplitude of the modulation. The behavior of the curve associated with a pressure of 5 MPa at the crack tip may also be interpreted along the same line. Of interest is also the observation that the two curves appear to converge towards each other as the size of the crack increases. This result is further confirmed by those obtained if the decay length is decreased to become $\ell = 0.1$ mm, as shown in Figure (6b). On the other hand, the predictions concerning a dry surface-breaking crack, which is partially closed by the same pressure field (see Figure (6a)), do not present features which significantly differ from those already shown in Figures (4a) and (5a). Finally, worthy of attention is the difference between the values of the plateau in Figures (5b) and (7b), the former being slightly larger than the latter (1 versus 0.75). This finding may be expected in virtue of the positive correlation between the values of ℓ and the extent of the region over which a significant variation of the local stiffness takes place. That is to say, the wider this region, the stronger the effect of the modulation on the amplitude of the backscattered wave, the extreme case being that considered in Figure 4 for $P_{tip} = 5$ MPa.

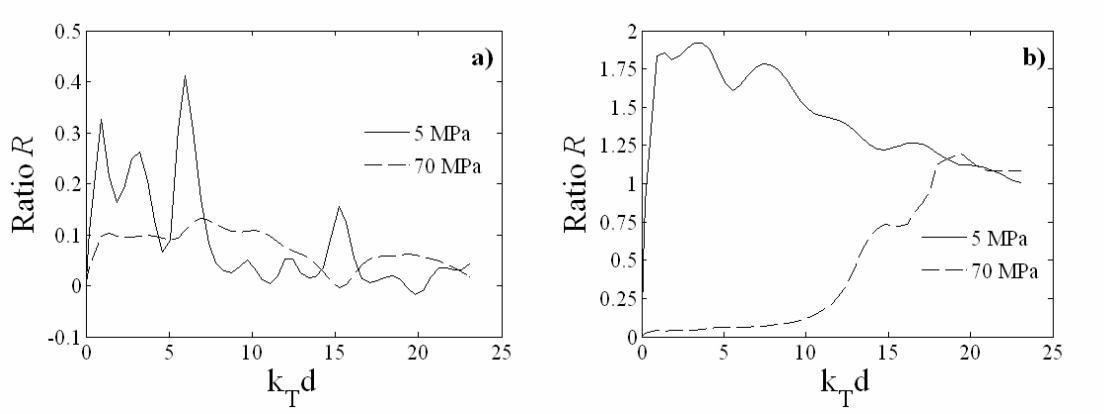

Figure 5. *Ratio, R, versus nondimensional crack size $k_T d$ for values of the pressure at the crack tip equal to 5 MPa and 70 MPa. The pressure distribution decays exponentially from the crack tip with a characteristic length ℓ=1 mm: a) dry surface-breaking crack, b) water-confining surface-breaking crack.*

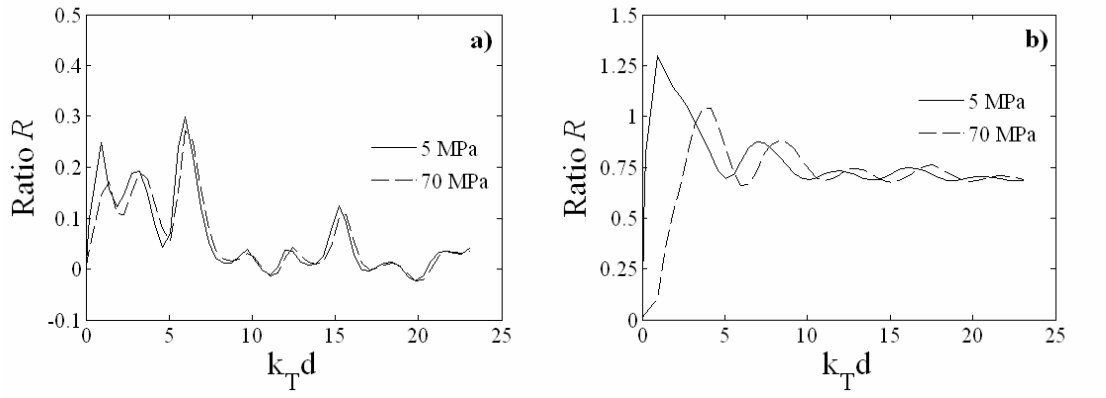

Figure 6. *Ratio, R, versus nondimensional crack size $k_T d$ for values of the pressure at the crack tip equal to 5 MPa and 70 MPa. The pressure distribution decays exponentially from the crack tip with a characteristic length ℓ=0.1 mmt: a) dry surface-breaking crack, b) water-confining surface-breaking crack.*

The investigation carried out on a surface-breaking crack has been repeated with a subsurface crack. Contrary to the former case, the investigation on the latter yielded results which do not substantially differ from each other. For this reason, only the predictions on the dependence of the ratio R on the size of a crack subjected to a pressure field decaying with a constant ℓ = 1 mm are presented next, those in Figures (7a) being obtained for P_{tip} = 5 MPa, while P_{tip} = 70 MPa in Figure (7b). Each figure illustrates the behavior of R for three values of the ligament size: a/λ_T = 0.4, 1 and 2. The most relevant feature of these results is that, with the exception of a small range of values of

$k_T d$ corresponding to cracks smaller than one wavelength of the incident wave, the ratio R remains always below a threshold value of 0.3.

In view of earlier results proving the higher sensitivity of shear waves to small surface breaking cracks when they are insonified at angles of incidence just above the critical angle of longitudinal waves [Pecorari and Poznic 2005, Pecorari 2005], the behavior of the ratio *R* has been examined also under these conditions, and found to yield no clear criterion to discern subsurface from surface-breaking cracks. Similar negative results have obtained with longitudinal waves at 45 degrees, 60 degrees and 85 degrees incidence.

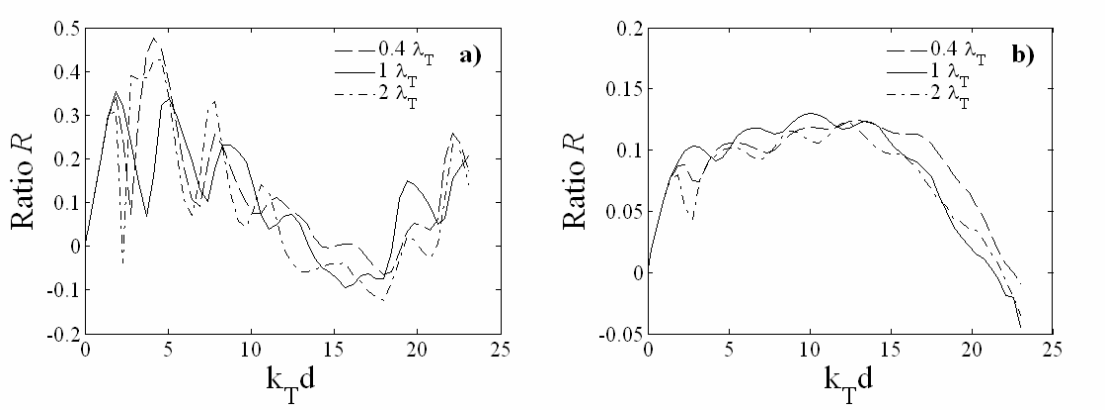

Figure 7. *Ratio, R, versus nondimensional crack size $k_T d$ for values of the ligament equal to $0.4\lambda_T$, $1\lambda_T$, and $2\lambda_T$. The pressure distribution decays exponentially from the crack tip with a characteristic length ℓ =1 mm: a) P_{tip} = 5 MPa, b) P_{tip} = 70 MPa.*

Finally the results in Figure (8a,b) concern the sensitivity of the ratio *R* to a variation of the angle on incidence from 45 degrees to 40 degrees, both for a surface-breaking crack which is filled with water (a), and for a dry subsurface crack (b). The pressure closing the crack is characterized by P_{tip} = 70 MPa and ℓ = 0.1 mm, which is the less favorable of the two cases. Similar results have been obtained for an angle of incidence equal to 50 degrees and by reducing the value of the pressure at the crack tip to 5 MPa. The main conclusion to be drawn from the latter results is that the proposed technique appears to be robust within a variation of the angle of incidence of at least ± 5 degrees.

Summary and concluding remarks

The potential use of the modulation technique to discern surface-breaking from subsurface cracks in components carrying pressurized water has been investigated theoretically. To that end, a model predicting the backscattered signal from dry and water-confining surface-breaking cracks and from subsurface cracks has been developed.

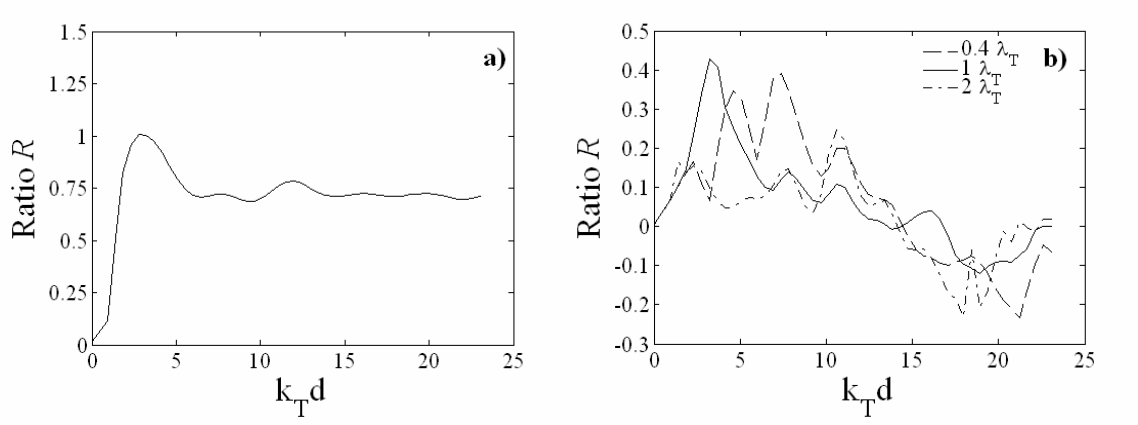

Figure 8. *Ratio, R, versus nondimensional crack size k_T. The pressure distribution decays exponentially from the crack tip with a characteristic length ℓ=0.1 mm, and P_{tip} = 70 MP. a) Water-confining, surface-breaking crack, subsurface crack with ligament size equal to 0.4λ_T, 1λ_T, and 2λ_T.*

By using the backscattered signals recorded at the two turning points of a modulation cycle, $B^{-,+}$, and when the no modulation is applied, B_o, the ratio $R = \left(B^- - B^+\right)/B_o$ has been constructed which does not depend on the amplitude of the incident wave, though it appears to vary with both angle of incidence and wave polarization. For a shear vertical wave at 45 degree incidence, R is predicted to exceeds a threshold limit of 0.5 when a surface-breaking crack is filled with water, while it is always lower than 0.5 if the crack, whether surface-breaking or subsurface, is dry. The difference in the values of the ratio is ascribed to the dramatic variation of the normal stiffness of a partially closed, water-confining crack as the surfaces of the latter come into contact, and it may be used as a criterion for differentiating water-confining surface-breaking from subsurface cracks.

To confirm the validity of the proposed method a deeper investigation into the role of the rms roughness of the composite interface formed by the crack surfaces needs to be carried out. In fact, as illustrated in Pecorari and Poznic [2005], the variation of the

normalized normal stiffness of a water-confining interface is considerably reduced when the rms roughness of the interface increases from 0.1 μm to 1.5 μm. However, results by Parisi *et al*. [2000] (and references therein) which are relevant to this issue need also be taken into account if the profile of a stress-corrosion crack displays self-affine properties like that of a fatigue crack. Should this be the case, in fact, the extent to which a self-affine profile can be represented by models describing the statistical properties of an infinite interface treated as a stochastic process with infinite spectrum must be reassessed. Of relevance to the behavior of the partially closed crack tip and to the model used to predict its acoustic response is also the asymptotic behavior of the normal stiffness in proximity of the crack tip. In this work, the crack is assumed to be either uniformly closed or increasingly open as the observation point moves from the tip toward the mouth of the crack. Watanabe *et al.* [2005] have recently brought to the authors' attention the incompatibility between the asymptotic behavior of the stress $\left(\propto \sqrt{1/r}\right)$ and of the displacement discontinuity $\left(\propto \sqrt{r}\right)$ when the crack stiffness is assumed to be constant and finite. This incompatibility would be removed if the self-affine nature of the crack surfaces were considered. In fact, the rms roughness evaluated over an interval shorter than the smaller cut-off wavelength of the profile's power spectrum, and including the crack tip would be zero. Thus, the crack would be either completely open or completely closed in a neighborhood of its crack tip. In the first case $K_N = 0$, in the second $K_N \to \infty$, and in both the use of the spring boundary conditions would result to be compatible with the assumed asymptotic behavior of the quantities involved. However, whether either condition would extent far enough from the crack tip to affect the numerical solution of the scattering problem obtained in this work remains a matter to investigate. The limits of the model notwithstanding, it is the authors' opinion that the proposed method deserves the consideration of a working hypothesis for further experimental investigation, which, alone, can provide a definite answer to the problem of interest to this communication.

Acknowledgments

This work was carried out as part of the project entitled "Detection of stress-corrosion cracks by means of nonlinear scattering of ultrasonic waves" which is sponsored by the Swedish Centre for Nuclear Technology.

References

J.D. Achenbach, L.M. Keer, and D.A. Mendelsohn, "Elastodynamic analysis of an edge crack", *J. Appl. Mech.* **47** (1980), 551-556.

J.M. Baik and R.B. Thompson, "Ultrasonic scattering from imperfect interfaces: a quasi-static model", *J. Non-Destr. Eval*. **4** (1984), 327-344.

A. Baltazar, S.I. Rokhlin, and C. Pecorari, "On the relationship between ultrasonic and micromechanic properties of contacting rough surfaces", J. of Mech. Phys. Solids **50** (2002), 1397-1416.

R.J. Brind, and J.D. Achenbach, "Scattering of longitudinal and transverse waves by a sub-surface crack", *J. Sound and Vibration* **78** (1981), 555-563.

S.K. Das, M.M. Sharma, and R.S. Schechter, "Solvation force in confined molecular fluids using molecular dynamic simulation", *J. Phys. Chem*. **100** (1996), 7122-7129.

B.W. Drinkwater, R.S. Dwyer-Joyce, and P. Cawley 1996 A study of the interaction between ultrasound and partially contacting solid-solid interface", *Proc. Roy. Soc. Lond. A* **452** (1996), 2613-2628.

A. Grabbe, and Horn R.G., "Double-layer and hydration forces measured between silica sheets subjected to various surface treatments", *J. Coll. Interf. Sc*. **157** (1993), 375-383.

J.-Y. Kim, V.A. Yakovlev, and S.I. Rokhlin, "Surface acoustic waves modulation on a partially closed fatigue crack", *J. Acoust. Soc. Am.* **115** (2004), 1961-1972, and references therein.

J.-Y. Kim, A. Baltazar, and S.I. Rokhlin, "Ultrasonic assessment of rough surface contact between solids from elastoplastic loading-unloading hysteresis cycle", *J. of Mech. Phys. Solids* 52 (2004), 1911-1934.

J.N. Israelachvili, *Intermolecular and surface forces*, 2nd edn. Academic Press, London, 1992.

A. Jenssen, K. Norrgård, R. Lundström, B. Claesson, and H. Ericsson "Metallographic examination of cracks in nozzle to safe-end weld of alloy 182 in Ringhals 4", Studsvik Report, Studsvik/N(H)-00/099 (2000).

V.V. Kazakov, A. Sutin, and P.A. Johnson, "Sensitive imaging of an elastic nonlinear wave-scattering source in a solid", *Appl. Phys. Lett.* **81 (**2002), 646-648.

R. Ho, J.-Y. Yuan, and Z. Shao Z., "Hydration force in the atomic force microscope: a computational study", *Biophysical Journal* **75** (1998), 1076-1083.

D.A. Mendelsohn, J.D. Achenbach, L.M. Keer, "Scattering of elastic waves by a surface-breaking crack", *Wave Motion* **2** (1980), 277-292.

P.B. Nagy, "Ultrasonic classification of imperfect interfaces", *J. Non-Destr. Eval*. **11** (1992) 127-140.

J.A. Newman, W.T. Riddell, and R.S. Piascik, "Analytical and experimental study of near-threshold interactions between crack closure mechanisms", NASA/TM-2003-211755,ARL-TR-2774 (2003).

A. Parisi, G. Caldarelli, L. Pietronero, "Roughness of fracture surfaces", *Eurphys. Lett.* **52** (2000), 304-310.

R.M. Pashley, and J.N. Israelashvili, "Molecular layering of water in thin films between mica surfaces and its relation to hydration forces", *J. Colloid and Interface Science* **101** (1984), 511-523.

C. Pecorari, "A note on the sensitivity of SV wave scattering to surface-breaking cracks", *Ultrasonics* **43** (2005), 508-511.

C. Pecorari, and M. Poznic, "Nonlinear acoustic scattering by a partially closed surface-breaking crack", *J. Acoust. Soc. Am.* **117** (2005), 592-600.

C. Pecorari, and M. Poznic, "On the linear and nonlinear acoustic properties of dry and water-confining elasto-plastic interfaces", to appear in *Proceedings of the Royal Society A: Mathematical, Physical and Engineering Sciences*.

S.I. Rokhlin, L. Wang, B. Xie, V.A. Yakovlev, and L. Adler, "Modulated angle beam ultrasonic spectroscopy for evaluation of imperfect interfaces and adhesive bonds", *Ultrasonics* **42** (2004), 1037-1047.

K. Watanabe, S. Ueda, S. Biwa, private communication (2005).

H. Xiao, and P.B. Nagy, "Enhanced ultrasonic detection of surface-breaking cracks by laser-induced crack closure", *J. Appl. Phys*. **83** (1998), 7455-7460.